Nanoscale Horizons

REVIEW

Published on 12 May 2025
Licence and permissions

Check for updates

Cite this: *Nanoscale Horiz.*, 2025, **10**, 1542

Wearable biosensors for health monitoring: advances in graphene-based technologies

Mohamed A. Abdelfattah, [ab] Sina S. Jamali, [ab] Navid Kashaninejad [ac] and Nam-Trung Nguyen *[ac]

The human body is an intelligent system, continuously generating signals that correlate with specific vital activities and indicate the state of our health and fitness. Therefore, accurate and real-time tracking of these signals is important for monitoring our health and timely medical interventions. The quantification of these signals in real-time is made possible by using skin wearable devices that detect disease-related biomarkers in bodily fluids, such as sweat and interstitial fluid. Integrating nanomaterials, particularly graphene, into wearable devices has dramatically enhanced the performance of wearable biosensors. The exemplary electrical properties, mechanical flexibility, and biocompatibility of graphene have made it a revolutionary material to shape the future of wearable devices. Graphene is versatile because its surface chemistry can be easily tuned to accommodate different biorecognition elements. This review provides an overview of flexible wearable biosensing devices, their sampling methods, and how microfluidic approaches enhance their performance. The paper also discusses the different strategies for the synthesis of graphene nanostructures, their integration into wearable systems, and their ability to improve sensing performance. Various surface chemistry modification techniques are also explored for the enhancement of the immobilisation of biomolecules. Finally, the paper discusses the challenges of graphene-based wearable technologies and their roles in continuous health monitoring and personalised medicine.

Received 11th March 2025,
Accepted 9th May 2025

DOI: 10.1039/d5nh00141b

rsc.li/nanoscale-horizons

Introduction

Wearable biosensors allow users to monitor their health conditions. This technology enables continuous health monitoring, improving disease management, prevention, and timely medical intervention.[1] A wearable sensing system is an integrated analytical tool that combines point-of-care (PoC) features with wireless connectivity, operating independently as an autonomous system. These devices continuously monitor an individual's physiological and biochemical data non-invasively or with minimal invasiveness. This approach enables the surveillance of subtle physiological fluctuations from baseline values throughout an extended period of time.[2] Wearable technology has existed for decades. The Holter monitor, for instance, has measured heart activity since the 1960s and has evolved significantly.[3] Although wearable devices differ in their applications, they typically consist of the following standard components: substrates, electrode materials, sensors encompassing interfacing, biofluid sampling, analyte biorecognition, generation of signals and their transmission to the amplification components, followed by signal-analysis units that collect, process, and transmit data, as well as the power unit.[4]

Today's wearable technology can deliver measurements of a quality level comparable to that obtained from standard medical instruments. Hence, it is becoming difficult to differentiate between wearables targeting consumers and those certified as medical devices. Early wearables focused primarily on biophysical monitoring by measuring metrics such as body temperature, heart rate, physical activity, and weight. However, as these devices evolved, they covered other applications as well.[2,5] Owing to the wide adoption and success of early wearables, the emphasis has increasingly shifted to more efficient, continuous, non-invasive or minimally invasive monitoring approaches, representing a significant stride towards personalised healthcare solutions.[6,7] Second-generation wearable devices include on-skin tattoos, patches, tooth-mounted films, smart textiles, contact lenses, and more invasive options like microneedle-based and injectable devices.[8–10]

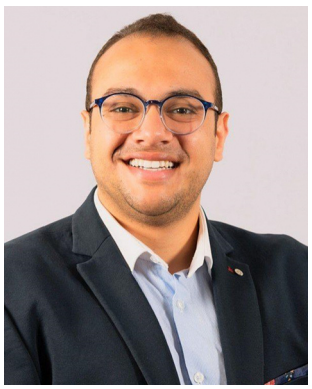
Several factors must be thoroughly considered when designing and fabricating a functional wearable device. Consistent and reliable performance is crucial for high-quality devices. In

[a] *Queensland Quantum and Advanced Technologies Research Institute, Griffith University, Nathan, QLD 4111, Australia. E-mail: nam-trung.nguyen@griffith.edu.au*
[b] *School of Environment and Science, Griffith University, Nathan, QLD 4111, Australia*
[c] *School of Engineering and Built Environment, Griffith University, Nathan, QLD 4111, Australia*

This journal is © The Royal Society of Chemistry 2025

addition, cost-effectiveness and biocompatibility with skin and body fluids are vital if a sensor is considered commercially viable.[11] The choice and preparation of materials are instrumental in creating high-quality flexible sensors. This includes the selection of appropriate flexible substrates and conductive filler materials. Material selection and preparation are critical to manufacturing flexible sensors. These materials must retain high conductivity, flexibility, and durability that can hardly be offered by the conventional sensing electrodes used for the past decades.[12] The exceptional mechanical properties of such materials are essential for fabricating wearable devices, providing excellent device stability with conformational changes.[13]

Therefore, nanomaterials have emerged as promising materials for sensing electrodes, taking over the conventional bulk electrode materials in flexible biosensors. The advances in medical sensor technology heavily depend on advances in nanomaterials.[14,15] Nanostructured materials, including carbon-based nanomaterials, conductive polymers, and metal nanoparticles, have been extensively studied for on-skin wearables owing to their biocompatibility and superior electrical, physical, and chemical characteristics, including their high carrier mobility rate, high thermal conductivity, extraordinary mechanical resilience, and expansive specific surface area.[16–19] These unique characteristics have been exploited in a wide



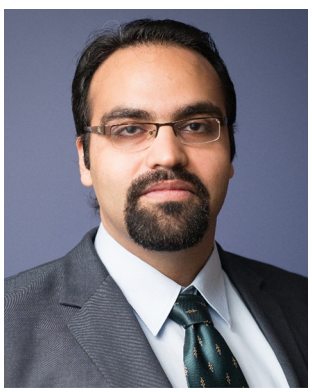
Mohamed A. Abdelfattah

Mohamed Adel Abdelfattah is a PhD candidate in Biomedical Engineering at the Queensland Micro- and Nanotechnology Centre, Griffith University, Australia. He previously served as a research assistant (2023) at the National Institute for Materials Science (NIMS), Japan. He holds an MSc in Biotechnology (2019) from the Egypt-Japan University of Science and Technology (E-JUST) and a BSc in Microbiology (2015) from Helwan University, Egypt. His current research focuses on developing next-generation graphene-based wearable biosensors for real-time monitoring of stress and mental health biomarkers.



Sina S. Jamali

Sina Jamali is an ARC DECRA Fellow and Senior Lecturer at Griffith University, where he leads a research group within the School of Environment and Science. He received his PhD from the University of Wollongong in 2016 and has held academic, industrial, and fellowship positions at the University of Wollongong, UNSW Sydney, and various collaborative research centres. Dr Jamali is an established electrochemist with a track record in the development of electroactive materials and biosensing technologies. His research integrates materials chemistry, bioelectronics, and electroanalytical methods to advance next-generation biosensors with improved sensitivity, specificity, and operational stability.



Navid Kashaninejad

Navid Kashaninejad received his PhD from Nanyang Technological University (NTU), Singapore, under the prestigious SINGA scholarship. He has extensive experience in designing and fabricating microfluidic devices for biomedical applications, including cancer treatment. In 2021, he was awarded the DECRA fellowship, recognizing his significant contributions. Currently, he is pioneering the emerging field of surface microfluidics, working to establish and advance its applications. His research focuses on innovative fabrication techniques and complex surface interactions. These contributions are poised to make a substantial impact across a range of applications, from advanced microfluidic devices to cutting-edge biosensing technologies.



Nam-Trung Nguyen

Professor Nam-Trung Nguyen received his Dip-Ing, Dr Ing and Dr Ing Habil degrees from Chemnitz University of Technology, Germany, in 1993, 1997 and 2004, respectively. From 1999 to 2013, he was an Associate Professor at Nanyang Technological University, Singapore. From 2013 to 2023, he was a professor and director of Queensland Micro- and Nanotechnology Centre at Griffith University, Australia. In 2023, he was awarded the prestigious Australian Laureate Fellowship for advancing the field of microfluidics. He is a Fellow of ASME and a Senior Member of IEEE. He is also an Elected Fellow of American Society of Mechanical Engineers.

range of applications, including sensors, optics, biology, medicine, and energy storage.

Carbon-based nanomaterials, particularly graphene, enhance biosensor performance due to their exceptional properties.[20] Graphene is a two-dimensional (2D) single layer of carbon atoms arranged in a perfect honeycomb-like hexagonal lattice. This carbon allotrope is one of the most revolutionary materials of the past two decades, owing to its extraordinary electrical, mechanical, thermal, and optical properties.[21] Therefore, graphene has been extensively associated with various applications, such as electronics, optoelectronics, telecommunications, energy storage, healthcare, and biomedical applications.[22]

Graphene nanostructures possess unique characteristics for biomedical applications, including superior conductivity, electrochemical stability, large surface area, biocompatibility, mechanical durability, transparency, and cost-effectiveness.[23] These features make graphene a cornerstone material for a wide range of medical devices, including optical,[24] electrochemical,[25] and field-effect transistor (FET) biosensors,[26] artificial muscle and skin,[27,28] wearable human–machine interfaces,[29,30] and artificial throats.[31]

In recent years, graphene has garnered significant attention in the fields of digital health and portable bioanalytical wearable biosensors due to the unique combination of its properties.[32] Graphene has been recognised as an efficient material for wearable sensors because of its light weight, flexibility, high sensitivity, and capability of seamless integration with the human body, accommodating the body's conformational changes, while enabling precise monitoring of parameters of interest in real-time.[33] The detection of the relevant parameters is facilitated by graphene's extended surface, excellent electron mobility, and ability to detect minute changes in its environment, making it an ideal candidate for developing next-generation wearable sensing technologies.[34]

In this paper, we first provide an overview of the latest advances in wearable technology to highlight the need for functional materials in signal enhancement. This is followed by an introduction to graphene nanostructures as functional materials and their transformative role in advancing wearable systems in healthcare monitoring. This review explores different types of wearable devices, accessible biofluids, and their sampling techniques, as well as relevant signal transduction, enhancement, and analysis essential for designing and deploying wearable devices. Next, we discuss the properties of graphene nanostructures, the effective modification strategies of surface chemistry required for the conjugation of biomolecules, and various signal transduction mechanisms employed in graphene-based wearables (Fig. 1).

While graphene-based wearable biosensors have been widely reviewed, most existing literature provides broad overviews without a focused analysis on strategies that enable truly seamless and fully wearable applications. Additionally, the role of surface chemistry modifications in ensuring effective immobilisation of biomolecules has not been explored in depth. In this review, we focus on addressing these gaps by exploring graphene and its potential towards novel research strategies, enabling fully wearable applications, alongside an in-depth discussion on the modification of surface chemistry for stable and effective biomolecule immobilisation. In addition, we examine the fundamental elements of wearable sensors to identify current trends and challenges, and recommend the future trajectory of this field.

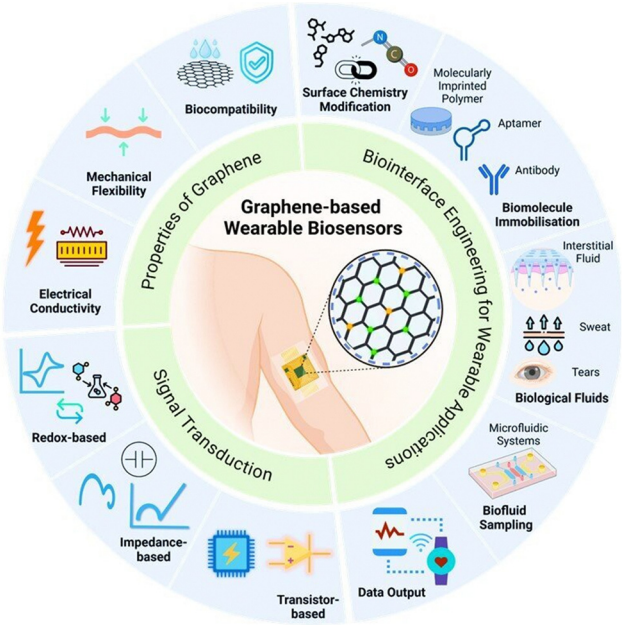


Fig. 1 Overview of graphene-based wearable biosensors and their application in healthcare, illustrating key properties of graphene, surface chemistry modification for suitable immobilisation of biomolecules, biofluid sampling strategies, and signal transduction mechanisms.

Wearable devices in healthcare management

Wearable sensors are emerging as a key solution to healthcare monitoring.[35] These in-home and point-of-care analytical devices are used to continuously monitor physiological and biological markers through non-invasive or minimally invasive methods. Compared to traditional point-of-care devices, which mostly rely on blood samples, wearable sensors can utilise easily accessible biofluids such as saliva, tears, and sweat to detect clinically significant biomarkers.[36] The ultimate goal of these devices is the continuous or regular monitoring process of clinically relevant parameters, allowing prompt intervention and preventative measures to be taken. Besides being designed with optimised mobility and accessibility, they should be compact, light, and autonomous, ensuring minimal impact on users' daily lives. A wearable device can be customised to deliver personalised healthcare tailored to each person, especially senior citizens and neonates.[37] Machine learning algorithms can be trained using the vast amounts of data they generate, which can be used in artificial intelligence to assist

 This journal is © The Royal Society of Chemistry 2025



Fig. 2 Examples of commercial wearable biosensors for continuous health monitoring. (a) *FreeStyle Libre* by Abbott for real-time blood glucose monitoring.[39] (b) *Dexcom G7* by Dexcom for advanced continuous glucose tracking.[40] (c) *Gx Sweat Patch* by Epicore Biosystems (Gatorade) for hydration and electrolyte analysis through sweat.[41,42]

decision-making.[38] Despite being expensive at present, these devices are expected to become more affordable in the future.

Wearables of the second generation have a prominent feature of using biofluids *via* biorecognition elements that transform the presence and concentration of particular analytes into measurable and quantifiable signals.[2] While most of these products are still in the prototype stage, a few notable commercial exceptions are illustrated in Fig. 2. Among the most popular wearables in the market for continuous glucose monitoring is the *FreeStyle Libre* (Fig. 2a),[39] and the *Dexcom G7* (Fig. 2b),[40] in addition to the *Gx Sweat Patch* for real-time hydration and electrolyte analysis (Fig. 2c).[41,42] In recent years, biophysical and biochemical wearable devices have been shown to be valuable tools for detecting and managing diseases and promoting wellness.[43] Moreover, wearable device applications extend beyond human-centric health and well-being, with their usage proliferating in monitoring the health of animals for both domestic pet care and animal livestock management purposes.[44]

State-of-the-art wearable sensors can provide reliable continuous monitoring of various vitals, including temperature, humidity, blood oxygen levels, blood pressure, electrogastrogram (EEG), and electrocardiogram (ECG). In addition, wearable sensors can access biofluids for monitoring and detecting clinically relevant biomarkers. The primary elements of wearable sensors include the sensing element and signal conditioning circuits. Analog-to-digital converters transform the analog signals into the digital format, while microprocessors or microcontrollers process the output into readable data. The acquired data are then stored in special memory units. Wireless communication modules then transmit the information. The device is usually equipped with a power source to supply the necessary energy for operation and interfaces.[36,45] Collectively, these elements enable monitoring and analysis of various physiological and environmental data, supporting applications in personalised healthcare and wellbeing.

The main goal of wearables is offering convenient and non-invasive means to track various biomarkers at home. To achieve their full potential, wearable devices should integrate all essential components mentioned above within a compact and functional system while enabling regenerated biomarker detection. Despite the significant advances in fabrication and testing methods of sensing platforms, the need for external analysers often conflicts with the core concept of integrated wearable systems. In this sense, much research must be oriented towards associating the sensing platforms with the required electronics and analysers in a compact and miniaturised form.[46–51]

Additionally, device regeneration is a critical feature that enables continuous operation of a wearable sensor. The regeneration efficiency depends directly on the biorecognition element immobilised on the surface, which must remain stable and active under non-physiological conditions to allow continuous biorecognition events to occur.[52] Various approaches have been introduced to enable a reversible reaction between the bioreceptor and the target analyte. These strategies, as illustrated in Fig. 3a–d, include: (i) engineered enhancements of the sensor surface, (ii) bond cleavage by chemicals, heat, pH shifts, or light, (iii) electrostatic repulsion, and (iv) magnetic manipulation.[53] For example, Gao's group presented a reusable wearable sensor to measure nutrients and metabolites continuously. An electric potential was applied for a short period (under 30 seconds) to achieve regeneration. During this restoration process, the electrode's surface is manipulated, releasing the bound analyte and restoring the sensor to its initial functional state.[54]

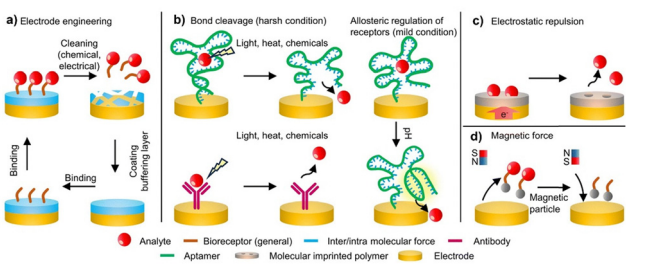


Fig. 3 Strategies for regenerable sensing. (a) Regeneration by electrode cleaning, either electrically or chemically, followed by buffer coating and immobilisation. (b) Regeneration by cleaving the biochemical bond with light, heat, or chemicals (left) and/or pH modulation (right). (c) Regeneration by electric fields, enabling electrostatic repulsion between the binder and the target molecule. (d) Regeneration by magnetic fields through a facile process of reversible removal and attachment of functional materials to the electrode. Reprinted with permission from ref. 53. Copyright © 2024, Royal Society of Chemistry.

A sensing platform is designed based on biorecognition events between the target analyte and the biorecognition element. In the biofluid, the target analyte interacts with the capturing element, which triggers changes in the device signal. This process enables qualitative and quantitative detection of the target molecule. In a standard biosensing surface, an electrode is immobilised with a biomolecule, which could be an antibody, aptamer, enzyme, peptide, or molecularly imprinted polymers (MIPs).[55,56] Choosing the correct biorecognition elements in wearable sensors is challenging because they must withstand extreme conditions. Antibodies and enzymes are not well suited because they are easily degraded outside their physiological context.[57] Currently, MIPs and aptamers are commonly used because they are highly resilient under non-physiological conditions and can be easily regenerated.[53,58] Since wearable devices are designed to track different biomarkers continuously, the regeneration capacity and biocompatibility of these recognition elements are of utmost importance.

For sensor fabrication, a substrate is initially functionalised with a bio-recognition element. Given that most wearable devices rely on electrochemical transduction for signal readout, the underlying substrate is usually an electrode.[59] Modifying the substrate successfully is crucial for the design of biosensors. Accordingly, the ideal electrodes must allow efficient and straightforward chemistry with the biomolecule, biocompatibility, resistance to fouling, and exhibit superior electron mobility for efficient signal transduction.[60] Following the modification of surface chemistry, the high affinity of the electrode towards the selected biomolecule facilitates the proper bioimmobilisation on the electrode surface. In order to improve the device sensitivity and overall performance, nanomaterials, including carbon allotropes, have been employed to develop novel electrode materials. This is due to their exceptional optical and electrical properties, high surface-to-volume ratio, and high affinity for efficiently immobilising bio-recognition elements. Specific nanomaterials have been used to generate signals from electrically active metabolites, including amino acids, ions, and other compounds.[61]

The substrate itself is also crucial to the sensing platform. It is imperative that the material on which the wearable sensor is constructed be both flexible and soft to conform to human skin. For this purpose, a variety of materials have been investigated. Polydimethylsiloxane (PDMS) has been widely used for various applications due to its ease of handling, versatility, moldability, and potential for creating microfluidic channels, as well as its softness and flexibility when applied to the skin. PDMS has been employed to fabricate a sweat-based sensor for cortisol measurement. This method involved the deposition of a gold electrode on a PDMS substrate and the creation of microfluidic channels within to deliver biofluids to the sensing chamber.[62] Another low-cost, flexible substrate is polyimide (PI). In spite of the fact that polyimide surfaces are not as soft as PDMS, they can be directly modified and used as electrode materials. For example, the Gao group showcased that lasers can modify PI surfaces to generate laser-induced graphene (LIG). This material can serve both as an electrode material and a substrate. Their study highlighted the use of LIG electrodes to detect cortisol in serum and sweat.[63]

Biofluids and sampling routes

Wearable biosensors are usually on-skin devices worn continuously to properly monitor an individual's physiological and/or mental state. In this regard, wearables must be comfortable, compatible, and conformal with the soft characteristics of the human body. Accordingly, extensive studies have recently been carried out on flexible wearable patches that can easily adapt to the human skin surface or be embedded into textiles. Additionally, biosensors should be utilised to monitor engaging and actionable parameters. Therefore, extensive research has been conducted to improve the measurement of vital signs by monitoring biochemical markers.[64] A wide range of body fluids can be assessed for biomolecular analysis. An ideal biological fluid collection or sampling procedure should be minimally or non-invasive, comprise a wide analyte diversity, correlate with relevant biomarker concentrations in blood, and precisely reflect the transient oscillation in biomarkers of interest.[65] Various sources of target analytes exist, such as interstitial fluid (ISF), sweat, saliva, urine, tear fluid, and breath. However, epidermal biomonitoring systems utilising two readily accessible biofluids, ISF and sweat, have been found promising as they are the most accessible biofluids for easy sampling. The precise and reliable non-invasive measurement of analytes in these biofluids has the potential to enhance a broad range of healthcare applications significantly.[66]

ISF exists between the cells and structural elements of the tissue. It resides in the extracellular space. Usually, it enters tissues from capillaries and then travels through the lymphatic system to return to the vascular system. The ISF can, therefore, be viewed as a fraction of blood plasma that is refined and free of cells. ISF is also regarded as an excellent source of biomarkers for biosensing since it exhibits comparable metabolomic and proteomic profiles to blood. Additionally, ISF can be accessed with a considerably lower level of invasiveness than blood, rendering it a suitable biofluid analyte to be monitored continuously with wearable sensors. The ISF may contain essential disease biomarkers that do not usually exist in the blood.[67] The primary methods for sampling ISF are microneedle and iontophoretic extraction techniques. Over several decades, these sampling techniques have been developed extensively, leading to their availability in various commercial products.[68]

Microneedles (Fig. 4a), comprising biocompatible microscopic needles that are fabricated from biologically inert hydrogels or synthetic polymers, are engineered to transverse from the stratum corneum through to the stratum basale of the epidermis to ultimately reach the dermis layer.[69,70] In wearable devices, microneedles have evolved from being designed for drug delivery to being used for minimally invasive biofluid sampling. A variety of microneedle architectures is available, including hollow microneedles that extract the ISF or porous microneedles that absorb the surrounding fluid.[71] As an

 This journal is © The Royal Society of Chemistry 2025

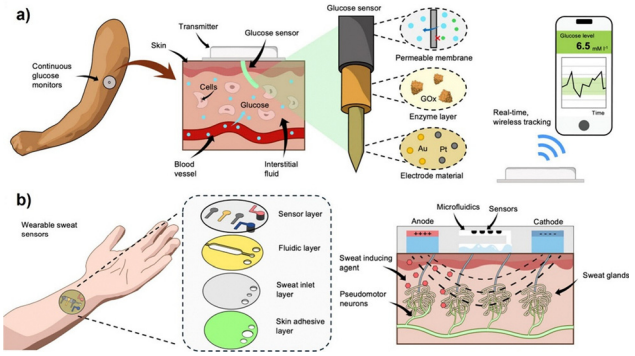


Fig. 4 Comparison of the minimally invasive ISF sampling and the non-invasive sweat sampling technologies for health monitoring: (a) schematic illustrating continuous biomarker monitoring, emphasising glucose detection in ISF by a minimally invasive microneedle-based sensor embedded in the interstitium. The electrode is made of conductive materials (gold or platinum) and modified with a permeable layer to avoid biofouling. It can detect glucose in ISF *via* the immobilised glucose oxidase layer, facilitating *in situ* real-time wireless measurement. (b) Schematic demonstrating the structure of wearable sweat sensors incorporating microfluidic layers for sweat sampling. The left figure shows the sensor's layers, including a skin adhesive layer with pores for sweat sampling, a sweat inlet and fluidic layers for transporting the collected sweat into the sensor layer where the biorecognition event occurs. The right side shows the process of sweat stimulation *via* iontophoresis, enabling continuous sweat release to ensure real-time monitoring. Reprinted with permission from ref. 70. Copyright © 2024, American Chemical Society.

alternative, solid microneedles can be used as penetration structures. Their surface can be utilised for optical or electrochemical analysis.[72] For instance, gold solid microneedles have been utilised for continuous real-time monitoring of drug levels in ISF. The sensor exhibited an aptamer-mediated electrochemical response that can be regenerated for multiple uses.[73] A microneedle device can be configured for continuous ISF sampling based on the application. However, this is usually for short periods, such as a few hours or a day. It is critical to optimise the mechanical strength of the microneedle patches to prevent buckling and fractures, close the prick wounds after the removal of the microneedle arrays, and address the local pain response during application.[74]

In iontophoresis, a mild electric current is applied to a specific skin area between an anode and a cathode. Consequently, charged molecules, such as sodium and chloride ions, migrate toward the cathode and anode, respectively. In addition to ions, uncharged molecules, including targeted biomarkers, are transported through convective mechanisms such as electroosmosis. Biomarkers move more efficiently across the skin due to electroosmosis. The skin's negative charge at neutral pH leads to a more excellent net transport to the cathode, which results in the preferential extraction of biomarkers at the cathode.[75–77] Concerning wearable sensing, it is worth mentioning that the electrode configuration and microfluidic sampling structures are designed to efficiently extract ISF from the body and transfer it to the external device *via* reverse iontophoresis.[78] Owing to its minimum invasiveness, iontophoresis is an ideal method for sampling ISF. A number of commercially available wearable devices, such as wrist-worn glucose monitors, depend on iontophoresis to withdraw ISF.[79]

There have been recent advances in iontophoretic-based wearables, such as thin layer-by-layer printing to produce micrometre-thin tattoo biosensors.[80] Using iontophoresis, on-demand or continuous detection can be achieved *via* electrical switching, enabling real-time sensing capabilities. Additionally, because iontophoresis is an electronic process, it is possible to integrate both sampling and sensing into a single system.[81] Nevertheless, prolonged use poses a challenge because the volume of fluid extracted is limited. The volume is determined by the applied current intensity. Elevated intensities of current potentially trigger discomfort, annoyance, and irritation. There has been an investigation of an alternative magnetohydrodynamic approach for non-invasive ISF extraction that provides faster extraction rates and reduces irritation compared to reverse iontophoresis.[82]

The majority of sensors developed for sweat analysis (Fig. 4a) have been designed primarily to detect metabolites to support fitness-related applications, with electrolytes, nutrients, and lactate serving as the most commonly studied analytes.[70,83] Sweat has attracted attention as a tool for monitoring glucose,[84] alcohol,[85] and cortisol.[58] Furthermore, sweat analysis has the potential to provide insight into a variety of pathogenic conditions, including cystic fibrosis,[86] viral infections,[87] and chronic inflammatory diseases such as inflammatory bowel disease,[88] and gout.[7] The presence of neuropeptide biomarkers in sweat can provide valuable information in assessing nervous system disorders.[89] While sweat is convenient as a biofluid, it presents several challenges regarding sample collection. In sweat collection, capillary wicking is often employed. Pores embedded in a synthetic polymer membrane are placed directly on the skin's surface to collect sweat.[90] Even though this approach is relatively straightforward, it has limitations, such as a small sample size. Hence, reverse iontophoresis is utilised as an alternative method of inducing sweat through active sweat induction.[10,91] Sweat-stimulating compounds are locally applied to the skin, followed by the extraction of sweat samples. Using this method, sweat and ISF samples can be collected into a single system, allowing for a greater range of biomarkers to be analysed and facilitating cross-correlations between different biofluid samples.[92] However, reverse iontophoresis approaches for sweat induction are subject to the same difficulties as the extraction of ISFs.

It is also possible to integrate wearable devices into face masks to sample and analyse non-invasively breath aerosols, which can carry biomarkers of respiratory pathogens.[93] Breath sensing technology is considered a potential tool for detecting and preventing diseases. However, technical challenges associated with its implementation include automating the collection of breath samples and integrating biosensors into an aqueous environment. The presence of over 3500 volatile organic compounds in breath is a challenge for the miniaturisation of such biosensors.[94] Furthermore, tear fluid possesses several unique protein biomarkers since it acts as a protective barrier. As a result, tear fluid is relevant for a wide range of

applications, such as the continuous monitoring of intraocular pressure in people with glaucoma and glucose levels in diabetics.[2] The use of contact lenses in diagnosing ocular diseases has been investigated. This type of biofluid sampling offers the advantage of being continuous and non-invasive, particularly when integrated into special contact lenses with augmented reality micro-displays.[3] Despite this, challenges exist in the miniaturisation of components: fitting into the strict geometry of contact lenses, on-eye sampling, inconsistency of tear production, and low correlation of tear production levels with blood levels.[94]

Furthermore, saliva-based diagnostic assays have recently been transitioned to wearable biosensing platforms. A number of wearable biosensors have been developed to detect glucose levels, including mouthguard biosensors. Others target oral diseases such as dental caries and periodontal disease using integrated wireless biodevices. Additionally, saliva diagnostics can be used to measure hormone levels to detect chronic pain, stress, and the use of illicit hormones.[95] Because saliva is continuously produced and non-invasive, it is a suitable monitoring biofluid for wearable devices. However, there are several challenges, including the high viscosity of saliva due to its mucin content, the variability in the kinetics of blood–saliva equilibrium, and interference from other oral activities. A saliva sampling device with inertial measurement sensors that can detect oral activity is being developed to address these challenges. Even though saliva sampling is convenient, long-term use of mouthguards or orally localised devices may be uncomfortable for the user.[43,96]

Another major diagnostic biofluid is urine. In the area of wearable technology, urine-based biosensing was primarily applied to diapers, where it was used to detect urinary tract infections and monitor glucose levels in diabetics.[97] Urine is a potential biofluid for biosensing owing to its non-invasive and easy sampling as well as the ability to be collected in large volumes. However, offering a proper application for urine sampling is challenging unless the device is integrated into diapers. In this sense, its application is limited to specific demographic groups, such as infants and the elderly, as well as patients in long-term care facilities. Additionally, the lack of nucleic acids and proteins in standard urinary output poses a challenge in detecting a broader window of diseases. Due to the nature of intermittent voiding events, such sensors are usually limited to performing a single analysis at a time, failing to provide real-time profiling of the targeted analyte.[95]

Microfluidic approaches for improved performance of wearable biosensors

In the early stage of the development of microfluidic devices, external equipment such as syringe pumps, pneumatic pumps, or peristaltic pumps is often used to control the flow of fluids. However, incorporating such pumping systems within microfluidic devices significantly increases their potential for commercial application since bulky external components are no longer necessary. As such, this technology provides advantages for developing integrated wearable microfluidic devices for enhanced and autonomous sampling of biological fluids like interstitial fluid, sweat, tears, saliva, and urine.[98]

These integrated systems are typically called soft micropumps, which can be categorised into active or passive micropumps. The latter usually relies on some inherent physical forces, including gravity, wettability gradients, surface tension, or hydrostatic forces. Therefore, these pumps do not need an external source of power. In contrast, active micropumps are powered by external energy sources, such as optical, electric, acoustic, piezoelectric, electromechanical, or magnetic energies. In wearable applications, active micropumps are ideal as they ensure controlled fluid flow and real-time adaptability.[99] For instance, straightforward finger-actuated micropumps are perfect for on-skin applications, as they need only one gentle pressure from the fingertip to trigger biofluid sampling into the microfluidic channels. This user-controlled and powered system ensures convenience and sustainability; it offers user discretion by enabling on-demand or intermittent sampling and testing, which is suitable for time-sensitive health conditions or interventions and sports tracking. A more sophisticated version may feature two or more actuation mechanisms, such as piezoelectric and electrohydrodynamic forces. Although these mechanisms require low-power external sources, they can achieve exact flow control for sensitive applications, such as controlled drug delivery.[100]

Integrating soft micropumps with flexible materials allows for the overall device's elasticity, enhancing its on-skin performance. The flexibility of microfluidic channels and pumps helps the device to automatically adapt to the skin while allowing smooth and continuous sampling of biological fluids. The collection and delivery of such fluids with stretchable materials is called micro-elastofluidics. A number of deformable materials have been investigated for micro-elastofluidics, including hierarchical bioinspired materials. Both organic and inorganic materials have been explored for the advancement of multifunctional and intricate micro-elastofluidic systems.[101] Modern materials science, along with soft robotics, are shaping the future of elastic microfluidic devices, which are classified according to their core materials into semiconductor-based, polymer-based, liquid metal-based, paper-based, and textile-based platforms.[102]

The most commonly used materials for micro-elastofluidics are polymers, including thermosetting and thermoplastic polymers, elastomers, thermoplastic elastomers, and hydrogels. For example, polyimide (PI) is an excellent thermosetting material for microfluidics and wearable applications. Its minimal creep and superior tensile strength make it highly resilient under mechanical, thermal, and chemical stress. Highly stretchable strain sensors with PI microchannels embedded with liquid metal demonstrated self-healing capabilities even after breaks in the microchannels, highlighting their potential for durable, on-skin application in demanding environments.[103] Another study reported the development of a microfluidic biosensor that utilises interdigitated microchannels fabricated on a Kapton substrate for the detection of heavy metal ions in polluted water samples.[104]

 This journal is © The Royal Society of Chemistry 2025

Paper-based microfluidic devices, also known as microfluidic paper-based analytical devices (μPADs), hold great potential for on-skin wearable applications. These devices have significant potential for commercialisation since they are compatible with electrochemical and optical assays, providing seamless real-time data insights. In recent studies, plasmonic devices with flexible, stretchable, and skin-conforming construction have been developed that can continuously sample and analyse sweat with surface-enhanced Raman scattering (SERS), providing non-invasive insight into physiological parameters.[105] In terms of feasibility, textile-based devices guarantee the highest flexibility and stretchability with the lowest fabrication complexity and cost, making them ideal for the fabrication of elastic wearable devices.[106] Recently, a group of researchers has engineered flexible electronic textiles by stitching liquid metal fibres into the fabric. The team used a sewing approach to integrate the fibres to make them more flexible and durable. A near-field communication (NFC) relay was incorporated within the fabric to enable seamless interconnection with smartphones while continuously monitoring the body temperature. The fabric was engineered to be washable for practical and sustainable use, ensuring its pliability and durability over washing.[107]

Signal transduction mechanisms for biomolecular sensing

Bioanalytical sensing primarily depends on biochemical interactions of bioreceptors and analytes, exploiting their specificity in detecting clinically relevant markers in bodily fluids. These biorecognition events are usually quantified and translated using various signal-transduction strategies, such as redox-based, impedance-based, and transistor-based sensors, Table 1. Such techniques facilitate detecting and monitoring a broad spectrum of analytes, directly or indirectly, providing insight into the physiological state of the body.[108]

A variety of capturing agents, such as aptamers, antibodies, proteins, DNA oligos, and MIPs, can serve for biomolecular detection of biomarkers. Amongst these, aptamers are regarded as an up-and-coming class of recognition molecules. They are synthetic short single-stranded oligonucleotide or peptide sequences with exceptional stability and specificity for a wide range of biomarkers, including small ions and large macromolecules. Aptamers are typically designed through SELEX (systematic evolution of ligands by exponential enrichment), resulting in customised 3D structures with high affinity for their respective analytes.[112]

In aptamer-based biosensors (aptasensors), aptamers are first chemically immobilised onto the electrode surface, facilitating efficient binding to their target. These biorecognition events trigger conformational changes in the aptamer, which alter the electron transfer process between the electrode surface and the redox-active reporter molecule (often methylene blue). The change in electron transfer behaviour produces a different electrochemical signal that corresponds to the analyte concentration.[113] Aptasensors function primarily through either target-induced displacement or binding-induced conformational shift mechanisms. In the latter, the aptamer undergoes structural changes upon interacting, adjusting the distance between the electrode and the redox-active reporter, resulting in a different electron transfer rate. However, the former demonstrates altering the electrochemical signal, upon biorecognition interaction, owing to displacing a complementary strand carrying a redox-active tag.[114]

Redox-based biorecognition biosensors. The redox-based system is the fundamental and most commonly used electrochemical signal transduction method. This approach mainly depends on electron transfer events occurring on the electrode surface, where an oxidation–reduction activity is induced once a potential is applied to the medium. Upon biochemical interaction on the sensor surface, the electron transfer process takes place between the electrode surface and the redox-active probe, generating a measurable signal corresponding to the analyte concentration. These electrochemical signals are analysed either by amperometry or voltammetry.[115] The latter could operate with cyclic voltammetry (CV), differential pulse voltammetry (DPV), or square wave voltammetry (SWV). Typically, these sensors are designed with a three-electrode setup: a reference electrode (RE) maintains a steady potential throughout the reaction, a counter/auxiliary electrode (CE) lets charge flow through a closed circuit, and a working electrode (WE) triggers the response. The WE surface is commonly functionalised with biological receptors, including enzymes, proteins, antibodies, MIPs, aptamers, or deoxyribonucleic acid (DNA) oligos for selective binding with analytes.[116]

Multiplex biosensors are considered a revolutionary advancement in disease management as they can simultaneously detect multiple biomarkers at a time. For example, a

Table 1 Advantages and limitations of signal transduction mechanisms in biosensors

Signal transduction method	Principle of operation	Advantages	Limitations	Ref.
Redox-based method	Measuring electron transfer during oxidation–reduction reactions of analytes or labels	Highly sensitive, well-established, and compatible with various biomolecules	Requires redox-active species, prone to interference, and limited to specific targets	109
Impedance-based method	Detecting interfacial impedance changes upon biomolecular interactions at the electrode surface	Label-free detection, real-time monitoring, sensitive to surface changes	Complex data analysis, affected by solution conductivity, needs baseline stability	110
Transistor-based method	Modulation of electrical current in a semiconductor channel due to analyte binding at the gate interface	High sensitivity, possible miniaturisation, low power, and suitable for comprehensive device integration	Complex fabrication, potential signal drift, and environmental stability concerns	111

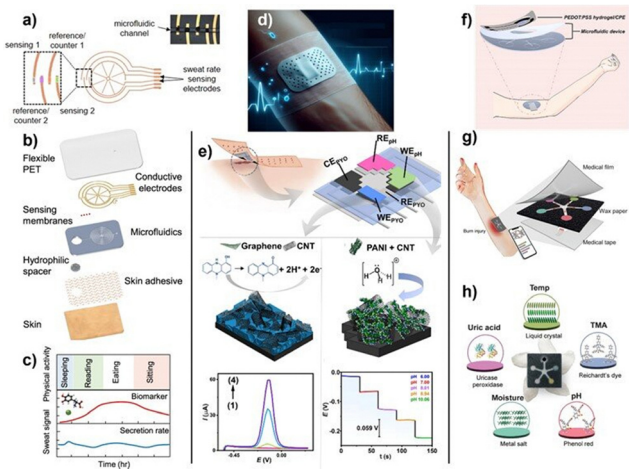


Fig. 5 (a) Electrochemical sensors for compositional analysis are functionalised near the tips of four semicircles and embedded within a microchannel. (b) Patch design featuring multiple layers: a skin adhesive interface collects sweat through hydrophilic fillers into microfluidics for measurement by sensing electrodes fabricated on a PET substrate. (c) Continuous monitoring of sweat secretion rate and composition over time without external stimulation is represented schematically by model trends. Reprinted under terms of CC-BY 4.0 from ref. 117. Copyright © 2021, Springer Nature. (d) Schematic illustration of a bandage-based sensor for direct wound status monitoring. (e) The structure of the sensors (top) and electrochemical sensing examples: SWV for pyocyanin detection at 0, 5, 50, and 100 μM concentrations using a porous CNT/graphene electrode (bottom left) and potentiometric pH sensor responses to various pH levels using a PANI/CNT composite electrode (bottom right). Reprinted under terms of CC-BY 4.0 from ref. 118. Copyright © 2024, Springer Nature. (f) Wearable microfluidic sensor integrated with the PEDOT: PSS hydrogel and carbon paste electrodes (CPEs). Reprinted with permission from ref. 119. Copyright © 2021, Elsevier. (g) PETAL sensor adhered to a burn wound for colourimetric analysis of wound healing, showing a layer-by-layer structure. (h) an absolute sensor patch resembling a five-petaled Pinwheel Flower (Tabernaemontana divaricata), and sensing principles for each colourimetric sensor (bottom). Reprinted under terms of CC-BY-NC 4.0 from ref. 120. Copyright © 2023, The American Association for the Advancement of Science.

multiplex electrochemical wearable sensor was developed to continuously analyse sweat at rest, addressing challenges associated with sweat dynamics like sweat evaporation and low secretion rates. The patches are designed to analyse sweat during sedentary and daily routines dynamically. The sweat rate sensor also assists patients with Parkinson's disease and hypoglycemia-induced sweating. Fig. 5a–c show the detection concept with integrated electrochemical sensors for real-time measurement of pH levels, chloride ions (Cl^-) concentration, and levodopa levels. Real-time measurement of sweat secretion rate is facilitated through hydrophilic fillers that are incorporated into the device. This patch enables continuous and non-invasive sweat analysis during rest, enhancing stress-tracking applications through sweat.[117]

Kaewpradub *et al.* reported a multiplex sensor to assess bacterial contamination associated with wound infections,[118] Fig. 5d and e. The device was developed to simultaneously detect pyocyanin, a bacterial virulence factor, and pH variability in wounds. The pH and pyocyanin sensors were screen-printed with inks made of porous polyaniline/multi-walled carbon nanotubes (PANNI/MWCNTs) and graphene/MWCNT composites, respectively, Fig. 5e.[113] Tracking microbial presence is essential for food safety, mainly through detecting toxins and other secondary metabolites produced by these microorganisms. For instance, a recent study has introduced electrochemical aptasensors for fungal aflatoxin B1 (AFB1) detection in food samples using a hybridisation chain reaction (HCR), a robust technique for signal amplification.[121,122]

Fenzl *et al.* reported a flexible LIG device with aptamer functionalised graphene to monitor thrombin and coagulation factor levels through a redox-based electrochemical reaction, achieving sensitivity down to 5 pM in complex serum.[123] Zhang *et al.* demonstrated the detection of thrombin levels in blood, allowing for real-time monitoring of blood coagulation status.[124] The device relies on gold nanoparticle (AuNP)-modified electrodes that are immobilised with DNA aptamers with a G-quadruplex-inducing structure. When thrombin binds to the aptamer, the latter forms the G-quadruplex structure, which changes the position of a methylene blue (MB) redox-active reporter, thereby altering the electron transfer rate. This conformational change in the aptamer and the resulting variation in electron transfer generate a characteristic electrochemical signal that accurately indicates the thrombin concentration. Xu *et al.* demonstrated the superior characteristics of hydrogels in enhancing sensitivity, electrolyte storage, and flexibility. The wearable device was fabricated using a poly(3,4-ethylenedioxythiophene) polystyrene sulfonate (PEDOT: PSS) hydrogel,[119] as shown in Fig. 5f. The device can detect and quantify uric acid (UA) in sweat for the management of gout and hyperuricemia.

Wearables are used not only for monitoring but also for therapy. These theranostic devices possess dual functional properties. For instance, Lee *et al.* developed a wearable multifunctional patch for both glucose sensing and drug delivery.[125] The amperometric sensor relies on detecting glucose in sweat through a chemical reaction with a glucose oxidase-decorated electrode *via* an oxidation reaction. This results in the production of hydrogen peroxide, which is detected electrochemically to reflect the glucose concentration in sweat. When it reaches a threshold, it triggers the release of the drug into the bloodstream. This wearable device not only ensures continuous glucose monitoring but also facilitates drug release through integrated microneedles for precisely controlled drug delivery. A redox-based concept could also serve as a colorimetric sensor, where a colour change is induced by either oxidation or reduction of a chromogenic substrate. Fig. 5g shows a paper-like PETAL sensor patch to monitor key wound healing parameters, including temperature, pH, and moisture levels, alongside trimethylamine (TMA) and UA, which are indicators of bacterial contamination and prolonged inflammation, respectively (Fig. 5h). The multiplexed sensors in this patch have been customised to operate with five independent colourimetric redox-based sensing mechanisms for a specific parameter.[120]

Impedance-based biosensors. In impedance-based biosensors, biorecognition interactions at the sensor's surface are

This journal is © The Royal Society of Chemistry 2025

measured and quantified using electrochemical impedance spectroscopy (EIS) as shown in Fig. 6a. EIS is a technique that determines the change in impedance within an electrochemical cell due to biochemical interactions through the biorecognition elements, as shown in Fig. 6b. The two types of impedimetric biosensors are faradaic and non-faradaic, which differ in their reliance on electron transfer reactions at the electrode interface. In Faradaic sensors, impedance is influenced by redox reactions occurring on the electrode surface. Such variation is directly proportional to the concentration of the target molecule.[126] Faradaic sensors are redox-based and contain an active redox probe that facilitates electron transfer to electrodes, corresponding to changes in charge transfer resistance (R_{ct}). The electrode interface characteristics and electrochemical kinetics changes are typically represented by Nyquist plots (Fig. 6c), which provide insights into electrode R_{ct} and the electrical double-layer capacitance (C_{dl}), modelled by the Randles equivalent circuit, Fig. 6d.

A non-faradaic electrochemical EIS system is considered the most promising tool for developing wearable real-time biosensors.[128] Non-faradaic impedance biosensors do not use redox labelling to measure impedance changes. No electrochemical reaction occurs on the electrode surface; instead, impedance changes are tracked through variations in the capacitance between the electrode surface and the formed electrical double layer. This variation in capacitance reflects changes in the sensor's dielectric behaviour upon biomolecular interaction.[129] The system setup of non-faradaic impedance biosensors typically relies on a single working electrode undergoing the reaction in a standard buffer solution of biofluid. The electrode is modified with the relevant recognition element without redox tagging to enhance selectivity and sensitivity toward target molecules. The processes of immobilisation and analyte detection spectroscopy are often carried out in the same solution, generating a spectrum represented by Bode plots, which provide information on impedance magnitude ($|Z|$) and phase shift (φ) and their dependence on the logarithm of the frequency.[130]

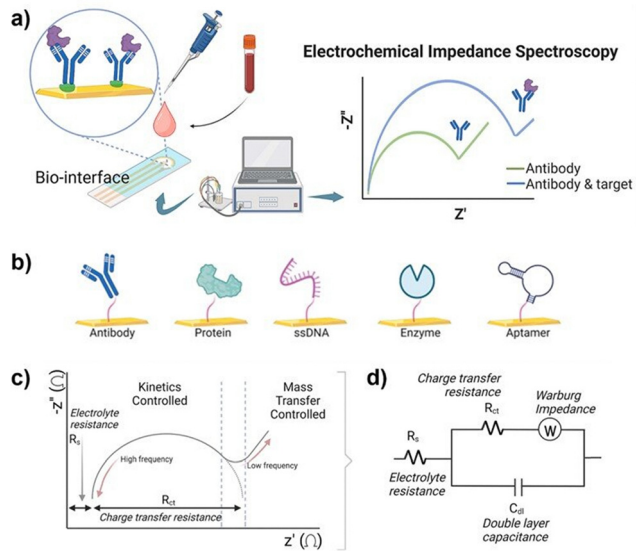


Fig. 6 (a) Schematic of an electrochemical setup, including the electrode-biological interface, an electrochemical workstation, and a representation of EIS data. (b) Illustration of various biorecognition elements used in biosensor development. (c) Nyquist plot showcasing the EIS response. (d) Corresponding Randles equivalent circuit model. Reprinted under terms of CC-BY 4.0 from ref. 127. Copyright © 2023, Elsevier.

The electrodes used in non-faradaic EIS sensing typically incorporate electrically conductive materials such as carbon-based materials, metals (silver, gold, and platinum), metal oxides, or conductive polymers. These materials are desired because of their superior electrical properties, stability in complex sensing environments, resistance to corrosion, and efficient electron transfer.[131] The electrodes commonly employed for this technique are interdigitated electrodes (IDEs). This design improves the detection of impedance changes and enhances the overall sensitivity and precision of the device.[132] Broader applications are made possible by this independence from redox-based reactions, especially in closed-loop systems, where redox-active species may obstruct the analyte detection process. Additionally, the non-faradaic method reduces the likelihood of interference and streamlines sensor design. For instance, some redox probes, such as ferro/ferricyanide electrolyte solution ($K_3Fe(CN)_6$ + $K_4Fe(CN)_6{\cdot}3H_2O$), show a high degree of toxicity and can denature proteins or interfere with other substances in complex media, which limits their applicability in the development of real-world bioanalytical devices.[133] Non-faradaic EIS biosensors are straightforward tools that are viable and practical for commercial applications. One prominent example is the glucose biosensor that detects changes in glucose levels in sweat. In this device, variation in impedance magnitude is brought on by glucose molecules' interaction with the glucose oxidase antibodies immobilised on the electrode interface. The electrode surface is made of zinc oxide (ZnO) and is responsible for the changes in the capacitance and resistance of the electrical double layer during the biomolecular interaction. This process can smoothly take place without the need for redox-active probes or the direct oxidation or reduction of glucose.[134]

The multiplexed EnLiSense's SWEATSENSER smartwatch is used for non-invasive continuous monitoring of interleukin-1β (IL-1β) and C-reactive protein (CRP) in sweat. The device employs a biofunctionalised screen-printed two-electrode system, facilitating the biomolecular interaction between IL-1β and CRP and their respective capture probe antibodies. The reaction produces a measurable non-faradaic EIS electrochemical signal that is used to measure the sensor response without redox tags. This device continuously tracks inflammation in people affected by inflammatory bowel disease (IBD), evaluating the efficacy of therapies and offering better disease management.[88] Similarly, an immunosensor based on single-walled carbon nanotube (SWCNT) electrodes was developed for non-faradaic EIS detection of interleukin-6 (IL-6). The electrode is functionalised by electrochemical deposition of AuNPs on the electrode surface to increase the overall device sensitivity and bioaffinity. This decoration of AuNPs facilitates efficient

immobilisation of IL-6-specific antibodies, which is crucial for binding to IL-6 antigens. Upon interaction, the electrode's R_{ct} is modulated, generating EIS signals that reflect the concentration of IL-6. The strong signalling and device performance are attributed to the high surface area and superior conductivity of SWCNTs, in addition to the electron transfer capabilities of AuNPs.[135]

Min *et al.* reported an autonomous wearable biosensor powered by a perovskite solar cell for real-time sweat sensing.[136] The device provides non-invasive and continuous insights into various parameters such as glucose, pH, sodium ions, sweat rate, and skin temperature, even under different lighting conditions. The device uses a flexible quasi-two-dimensional perovskite solar cell module that offers ample power under illumination without an external battery. Sempionatto *et al.* developed another multiplexed and integrated on-skin device for simultaneous monitoring of blood pressure and heart rate using ultrasonic transducers.[137] The device detects glucose, alcohol, lactic acid, and caffeine through non-faradaic electrochemical sensors. The device uses needleless iontophoretic extraction of ISF at the cathode, while pilocarpine is delivered at the anode for sweat stimulation.

Transistor-based biosensors. Designing transistor-based biosensors requires a unique setup for effective biomolecular interaction. Field-effect transistors (FETs) are the core of this sensing concept.[138] The sensing electrode serves as the gate of the FET, where bioreceptors, such as enzymes, antibodies, and aptamers, are immobilised to bind with the target analytes. When recognition occurs, the conductivity of the transistor channel changes with the minute binding events on the gate. Transistor channels are conductive pathways between the sensor's source and drain terminals. They are responsible for the sensitivity and are usually made up of high electron mobility semiconductor materials such as silicon nanowires, graphene, carbon nanotubes, metal oxide or organic semiconductors. Molecular changes lead to a change in the local electric field, thereby modulating the charge carrier flow between the source and drain. Changes in the current flow through the source and drain electrodes directly correlate with the concentration of the target analyte.[139]

An ion-sensitive field-effect transistor (IS-FET) can be potentially used for pH sensing and detecting target ions through a complementary functionalised gate surface. Variations in ion concentration near the gate affect the device threshold voltage at the semiconductor–liquid interface.[140] Another type is a silicon nanowire-based field-effect transistor (SiNW-FET) biosensor, which takes advantage of the superior properties of silicon nanowires, including the semiconducting properties and the high surface-to-volume ratio.[141]

Organic semiconductor-based FET (O-FET) biosensors rely on modulating the conductivity of an organic semiconductor channel when a target analyte is detected. The flexibility of organic semiconductors makes them ideal for wearable and implantable devices.[142] Applications of O-FETs hold a strong potential in on-skin diagnostic devices, as demonstrated by a recent study on recyclable and wearable organic electrochemical transistor (OECT) for detecting stress-related neurotransmitters. The sensor unit depends on functionalising the gate area with MIPs synthesised specifically to recognise epinephrine molecules.[143]

Metal oxide semiconductor FET (MOSFET) biosensors utilise an inorganic semiconductor base that can be easily functionalised. MOSFETs are electrically stable and highly sensitive, especially under complex conditions, unlike many OFETs, which show less stability in physiological environments. Materials such as indium oxide (In_2O_3), zinc oxide (ZnO), tin oxide (SnO_2), and titanium dioxide (TiO_2) are considered promising materials to be used either solely or in composites in MOSFET biosensors.[138] For instance, indium-gallium-zinc oxide (IGZO) was used to fabricate implantable biosensors embedded at the cellular interface to interact with live cells and provide real-time information.[144] For wearables, aptamers with stem-loop structures were employed to target hormones, namely dopamine and serotonin, in an In_2O_3 nanoribbon-based device, Fig. 7a–c. This allows simultaneous and sensitive detection for both biomarkers, with a 10 fM limit of detection for each neurotransmitter.[145] Fig. 7d–f show another on-skin In_2O_3-based transistor fabricated for aptameric sensing cortisol hormone, a key stress biomarker in sweat. Sweat is induced *via* an iontophoretic system integrated into the FET array in a smartwatch for seamless, continuous, and sensitive detection of cortisol with ultralow concentrations (1 pM).[146]

Graphene nanostructures are extensively used in making sensitive transistor-based bioanalytical devices by taking advantage of graphene's unique electrical and surface characteristics. Graphene-based FET (G-FET) biosensors demonstrated sensitive modulation of their electrical properties with minute biomolecular changes. Fig. 7j and i illustrate a graphene multi-transistor array (gMTAs), a good example of a G-FET's ultrasensitive detection of dopamine neurotransmitters in complex samples, like cerebrospinal fluid, with a limit of detection of 1 attomolar.[147] Another study reported a soft implantable G-GET (Fig. 7j–l) that was developed for real-time monitoring of dopamine *in vivo* with aptamers.[148] Zhang and Jia monitored cortisol levels in saliva using a liquid gate G-FET biosensor.[149] In this device, graphene thin films were inkjet printed on flexible PI substrates for the detection of cortisol concentrations ranging from 0.01 to 10^4 nM. Laliberte *et al.* reported a standalone wearable G-FET biosensor for aptameric detection of IL-6 protein in the range of 10 pM to 10 nM.[150]

Flexible graphene-based biosensors

Graphene, discovered in 2004, has transformed materials science and biomedical engineering due to its remarkable properties, such as high sensitivity, large surface area, superior electrical properties, and cost-effectiveness. Graphene is an attractive material for shaping the future of innovative diagnostic devices. These characteristics enable graphene-based devices to more precisely detect a wide range of physiological signals compared to other materials. Fig. 8 illustrates some of

 This journal is © The Royal Society of Chemistry 2025

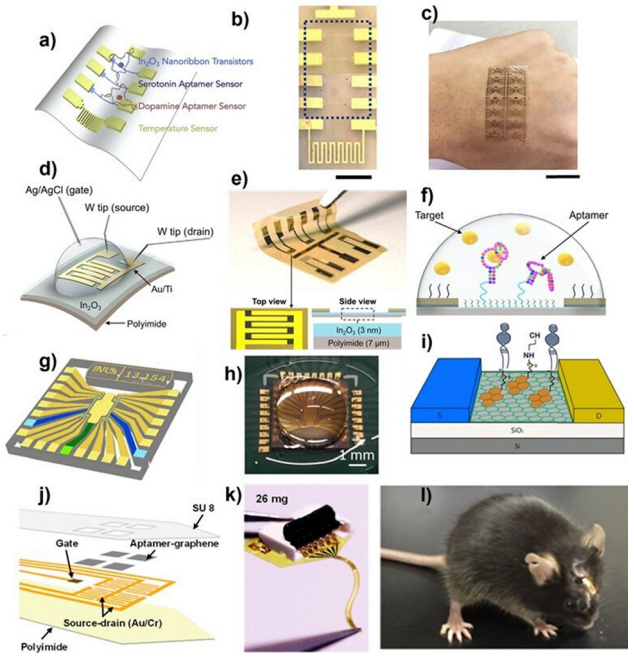


Fig. 7 (a) Schematic illustration of the wearable biosensor designed for monitoring serotonin and dopamine. (b) Optical microscopy image of a single device showing the Au common-gate electrode, four In_2O_3 nanoribbon FETs (dotted blue box), and an Au resistive temperature sensor (from top to bottom). The low contrast of the In_2O_3 nanoribbons is due to their transparency. Scale bar: 500 μm. (c) Flexibility of the sensor array, illustrated by its conformal attachment to human skin. Scale bar: 2 cm. Reprinted with permission from ref. 145. Copyright © 2020, Elsevier. (d) Schematic of the FET setup, where an Ag/AgCl reference electrode was used as the solution gate. The current between the Au/Ti source and drain electrodes was recorded with tungsten (W) probes. (e) Photograph of a FET sensor array with In_2O_3 semiconductor channels fabricated on a flexible polyimide substrate. Schematic layers are not to scale. (f) Schematic of the aptamer-FET sensing mechanism, illustrating cortisol-induced conformational changes in negatively charged aptamer phosphodiester backbones along with rearrangement of associated solution ions. Reprinted under terms of CC-BY 4.0 from ref. 146. Copyright © 2022, The American Association for the Advancement of Science. (g) Schematic illustration of one gMTA chip containing 20 electrolyte-gated graphene field-effect transistors (EG-gFETs) and corresponding interconnect lines and pads. (h) Photograph of a gMTA with a phosphate-buffered saline (PBS) droplet on top of the sensor area. (i) Schematic of fully functionalised graphene for each EG-gFET in the gMTAs. Reprinted under terms of CC-BY 4.0 from ref. 147. Copyright © 2022, Springer Nature. (j) Schematic illustration, and (k) optical image of the implantable aptamer-graphene micro transistor probe for neurological monitoring. (l) Image of a freely moving mouse implanted with the aptamer-graphene micro transistor probe. Reprinted with permission from ref. 148. Copyright © 2022, American Chemical Society.

the potential applications of graphene in implantable and wearable devices.[151]

LIG, introduced in 2014 by Lin *et al.*, has garnered considerable attention in recent years.[152,153] It represents a three-dimensional (3D) porous carbon nanomaterial synthesised *via* direct writing with a CO_2 laser on polymer substrates under ambient conditions. Alternate terminologies for LIG include laser-ablated graphene (LAG), laser-scribed graphene (LSG), or laser-derived graphene (LDG).[154] The morphological



Fig. 8 Current or future applications of graphene-based smart wearable and implantable devices. Reprinted with permission from ref. 151. Copyright © 2023, Elsevier.

characteristics of LIG are controllable through programmable laser parameters, offering significant implications for the advancement of highly sensitive electric/electrochemical sensors and wearable electronic devices. PI and its derivatives serve as common substrates for LIG fabrication, along other reported materials, including polyetherimide, potato skin wood, cork, coconut, fabric, and polysulfone.[155–157] The LIG synthesis process typically involves the use of an infrared CO_2 laser (usually emitting light with a wavelength of 10.6 μm).[158] Laser scanning of the polymer substrate disrupts nitrogen-carbon, carbon–oxygen, and carbon-hydrogen bonds, reorganising them into a 3D porous graphene network.[159] Beyond infrared CO_2 lasers, UV[160] has been explored for LIG fabrication.

Graphene architectures: fabrication pathways and structuring techniques

Pristine graphene is a pure, single-layered, non-defective lattice of carbon atoms arranged in a perfect 2D honeycomb structure. Graphene is characterised by its inertness, zero band gap, large specific surface area (2600 $m^2\ g^{-1}$), and ultra-thin structure (0.34 nm). Owing to its exemplary properties, besides having exceptionally unique thermal, electrical, and mechanical properties, graphene has revolutionised healthcare applications in the past 20 years. Depending on synthesis methods, graphene can be produced in various forms, including monolayer, few-layer (2–10 layers), and multilayer (>10 layers) graphenes. Initially, micromechanical exfoliation of bulk graphite produced monolayer graphene at the micrometre scale.[161] Graphene can be synthesised using chemical vapour deposition (CVD), a thin-film fabrication technique that involves introducing methane and hydrogen gases to chemically react in the presence of argon, serving as an inert gas carrier. This method is suitable for the large-scale production of high-quality metre-sized graphene monolayers. However, the application of monolayers in wearable devices is limited due to their fragility, thereby requiring additional protective structural designs to enhance their durability to conformational changes.[162]

On the other hand, few-layer and multilayer graphenes can be synthesised using liquid-phase exfoliation. The process involves breaking weak van der Waals (vdW) forces between out-of-plane carbon atoms of liquid-dispersed graphite by applying external forces, such as sonication or shear mixing.[163] Researchers used laser scribing as a promising method for growing multilayer graphene on commercially available polymers. These polymers, including polyetherimide (PEI), polyimide (PI), and sulfonated poly(ether ether ketone) (SPEEK), are used as a carbon source for graphene generation. For instance, PI was converted by CO_2 infrared laser engraving into porous multi-layered LIG with an average sheet resistance of 35 Ω sq^{-1}. For instance, Soares *et al.* employed CO_2 laser scribing to produce LIG electrodes on PI films, which were further functionalised with appropriate antibodies for detecting food-borne *Salmonella enterica* in chicken broth.[164]

High-quality LIG can also be generated using unconventional eco-friendly carbon sources like cork, wood, leaves, paper, nanocellulose, lignin, potato skins, and coconut shells, Fig. 9a–d.[165] This approach involves transforming the base material into amorphous carbon first, followed by a second laser scribing step to generate graphene. The produced graphene sheets typically contain defects and cracks, compromising the excellent properties of pristine graphene by inducing a bandgap in its electronic structure and increasing its chemical reactivity and mechanical durability.[166] Tuning these properties allows for the transition from a semimetal to a semiconductor, facilitating surface biofunctionalisation and enhancing its flexibility for functional adaptability, respectively. Hence, few-layered and multilayered graphene has the desired functionality and durability required for wearable applications.[167]

Graphene can be categorised into graphene-like derivatives such as graphene oxide (GO) and reduced graphene oxide (rGO). GO is a graphene nanoderivative consisting of single-layer sheets interspersed with sp^3-hybridised carbons and oxygen-containing functional groups. Typically, GO is synthesised by Hummers' method, through oxidising and exfoliating graphite precursors with strong acids and oxidising agents, including sulfuric acid (H_2SO_4) and potassium permanganate ($KMnO_4$), respectively. This method introduces oxygen functionalities between the graphite layers.[168] This method has been refined many times since the British scientist B.C Brodie first introduced it in 1859.[169] Since then, all emerging approaches have aimed for safer, quicker, and more efficient strategies to weaken the van der Waals forces between graphene layers within graphite and their exfoliation into dispersible single sheets. Since GO is a versatile material and precursor for other derivatives, many studies have been aiming to improve the oxidation process to make it more efficient and environmentally friendly. The abundance of oxygen-containing functional groups in GO is attributed to its hydrophilic nature, enabling its dispersibility in water and polar organic solvents.[170] These groups include hydroxyl and epoxide groups, which are polar and hydrophilic groups, on its basal planes, in addition to carboxylate groups at its edges, giving it a pH-dependent negative charge and stable colloidal form. These

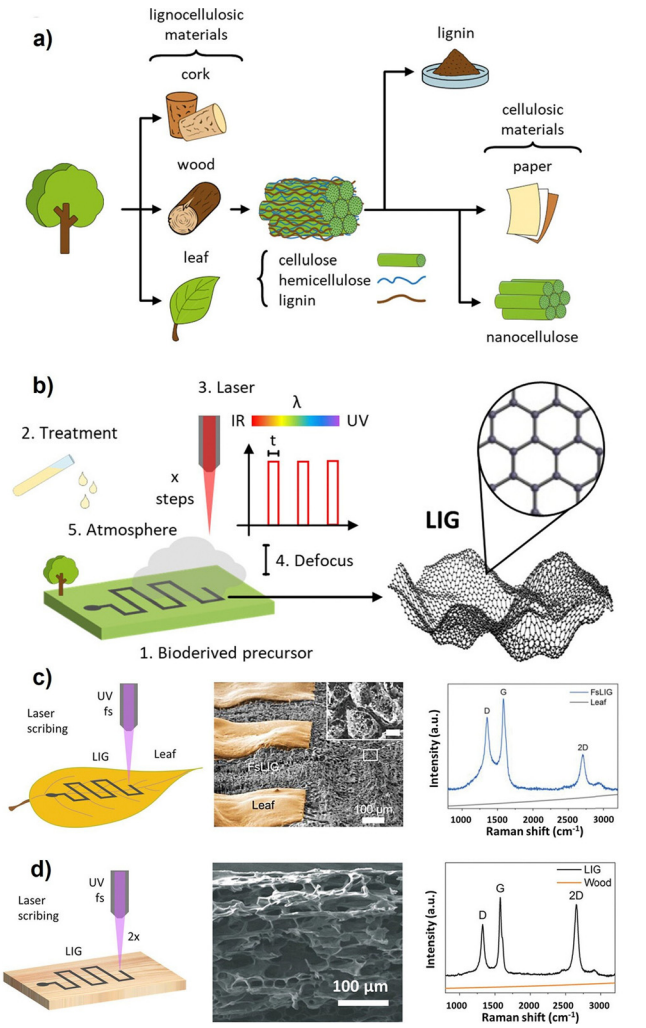


Fig. 9 (a) Schematic overview of the main eco-friendly precursors and their processing for graphene induction. (b) Laser scribing process of the processed bioderived materials. Factors influencing LIG induction: (1) chemical composition of the natural substrate; (2) surface treatment prior to engraving; (3) laser parameters: wavelength λ, pulse width and power, number of scribing steps x; (4) beam defocusing; (5) atmospheric conditions. SEM and Raman spectroscopy confirmed the UV/fs laser scribing process of (c) leaves and (d) wood. Reprinted under terms of CC-BY 4.0 from ref. 165. Copyright © 2023, Elsevier.

functional groups are crucial for GO's affinity to interact with a wide variety of biomolecules through covalent bonds, electrostatic, and other interactions. The chemical versatility, in addition to its large surface area, mechanical resilience, and biocompatibility, make GO and its derivatives suitable candidates for biosensing applications.[171]

Modification of GO produces derivatives with enhanced properties, namely reduced GO (rGO). The reduction process involves eliminating the oxygen-containing functional groups, including hydroxyl, carboxyl, epoxy, and carbonyl groups, and partially restoring the sp^2 carbon structure. However, pristine graphene will not be yielded after the reduction process, as there would be existing residual oxygen moieties and structural defects within the carbon lattice.[172] rGO is favoured in

This journal is © The Royal Society of Chemistry 2025

biomedical applications because of its enhanced electric conductivity, π–π stacking efficiency, bioaffinity, and hydrophobicity. Such enhancements enable loading hydrophobic biomolecules needed for biosensing applications. Reduction could take place in various ways, including chemical, thermal, biological, electrochemical, and photothermal reduction pathways. The reduced form of GO exhibits minimal oxygen presence, enhancing its properties, such as improved electron mobility, sheet conductivity, and higher physical interaction capabilities.[173]

Chemical reduction of GO is the most common method for rGO production. This method depends on hydrazine hydrate (HH) for a fast and efficient reduction. However, alternatives, such as sodium borohydride and L-ascorbic acid, are now preferred for GO reduction owing to HH's toxicity and hazardous properties.[174] In the case of thermal reduction, GO is exposed to elevated temperatures ranging from 200 °C to over 1000 °C in a vacuum or inert atmosphere.[175] Reduction can take place biologically through bacteria, especially *Shewanella oneidensis*, by utilising the oxygen moieties of GO in their unique respiratory extracellular electron transfer (EET) pathways. This electron transfer process is mediated by cytochrome proteins, including multiheme cytochrome *C* (MtrC) and outer membrane cytochrome A (OmcA), located in the bacterial outer membrane, ending with GO as a final electron acceptor.[176]

Both electrochemical and photothermal reduction techniques are environmentally friendly and are widely used for the *in situ* reduction of GO films. Electrochemical reduction occurs by applying a voltage across electrodes in an electrolyte solution, resulting in the removal of oxygen moieties from the GO surface.[177] Photothermal reduction is regarded as one of the most effective approaches for the mass production of rGO, transitioning from lab to industrial scale. Photothermal reduction is achieved by localised exposure of GO to a light source, resulting in the absorption of photons and subsequent heating of the GO surface. It is also believed that photochemical contributions are usually involved in the photothermal process since they provide the needed activation energy to selectively break chemical bonds of oxygen functionalities with an energy threshold of 3.2 eV. This process leads to removing oxygen functionalities and restoring the conjugated carbon network. It is usually associated with the emission of gases, which is typically attributed to a foam-like structure of the material. Generally, the light source could be a laser in the visible,[178] near-infrared (NIR),[163] ultraviolet (UV) light,[179] or solar light.[180] Laser irradiation, including CO_2 laser irradiation, is the most prominent type of photothermal *in situ* reduction of GO. For instance, CO_2 laser power, speed, and pulse per inch (PPI) were finely adjusted for efficient *in situ* reduction of GO films into laser-reduced GO films supported on polyethylene terephthalate (PET) substrates for flexible electronic applications.[181]

A laser-assisted strategy for the *in situ* modification of graphene could also achieve chemical doping. For example, conformal sulphur-doped LIG was created with a membrane of polysulfone-class polymers on the PI sheet.[182] Hamed *et al.* proposed real-time laser-assisted nitrogen doping and sulphur-nitrogen co-doping of rGO using ammonia solution and thiourea, respectively. The team found that the co-doped graphene showed superior electric properties over the other forms of graphene.[181] Wan *et al.* reported that laser irradiation of PI can result in self-doping of the porous LIG with nitrogen atoms, which increases the conductivity and sensitivity of biosensors.[183]

Micro- and nano-patterning methods of graphene. Lasers can be used to engrave graphene patterns, offering controlled modulation of sensors' designs to fit different applications. Laser patterning has gained attention for its simplicity, scalability for mass production, and direct writing capability on polymer substrates without the need for masks or complex cleanroom facilities.[184] Laser patterning has the advantage of rapid and simultaneous generation of porous and conductive graphene networks, suitable for electrochemical sensing applications. Such patterning is beneficial in enhancing the device's surface chemistry and electrical pathways, promoting the device's sensitivity, spatial resolution, and conformability to dynamic surfaces for a better wearable experience.[185] However, limitations include moderate resolution (~10–50 μm), potential edge roughness, and thermal degradation of the substrate due to the photothermal process.[186]

Photolithography remains the gold standard for patterning microelectronics, enabling high-resolution patterning (<1 μm) through UV exposure, photoresist masking, and subsequent etching. Photolithography offers excellent reproducibility and compatibility with multilayer designs.[187] However, this technique requires cleanroom facilities, harsh chemicals, and UV exposure. Furthermore, its application on flexible substrates is limited due to associated chemical, thermal, and mechanical stresses.[188]

Inkjet printing and aerosol jet printing are additive, maskless techniques that enable the direct deposition of graphene inks onto a variety of substrates, making them particularly attractive for wearable electronics. These approaches support scalable, low-cost, and on-demand fabrication of flexible and stretchable sensor arrays while minimising material wastage.[189] However, they are limited by relatively low resolution (~20–100 μm), challenges in ink formulation (*e.g.*, viscosity, dispersion stability), and often lower conductivity compared to CVD graphene unless post-treatment is applied.[190] On the other hand, microcontact printing and soft lithography using elastomeric PDMS stamps are used as an effective strategy for transferring graphene patterns onto flexible, delicate surfaces. These methods allow large-area patterning with gentle processing.[191] Nevertheless, they offer lower resolution (~1–10 μm) than conventional photolithography and may suffer from pattern deformation due to stamp softness, as well as alignment challenges in multilayer device fabrication.[192]

At the nanoscale, electron beam lithography (EBL) offers excellent precision for fabricating graphene nanoribbons and single-molecule sensors, achieving critical dimensions below 100 nm. This high-resolution technique is ideal for proof-of-concept studies and advanced sensor research, providing

accurate edge definition and enabling complex nanoscale architectures.[193] However, EBL is extremely slow, costly, and suffers from low throughput, making it unsuitable for mass production and commercialisation.[194] Some emerging technologies have appeared to address these limitations, including plasma etching, scanning probe lithography, and thermochemical nanolithography. These methods hold promising avenues for nanoscale patterning of graphene nanoderivatives while preserving their intrinsic properties and potentially improving process scalability.[195,196]

Graphene's wearable compatibility

Carbon-based nanostructures are one of the main building blocks in nanotechnology and have been extensively studied in developing flexible electrochemical biosensors. Their unique advantages include excellent electrical properties, large active surface area, high mechanical strength, superior thermal and chemical stability, and the presence of inherent structural defects that are needed for further functionalisation.[197] The most used carbon allotropes in electrochemical biosensing are pristine graphene, GO, rGO, and carbon nanotubes (CNTs). These nanomaterials play a crucial role in enhancing the performance of flexible sensors as they offer distinctive and exceptional physical properties.[198]

Mechanical robustness of graphene. The approximate thickness of the graphene monolayer is 0.335 nm, which can vary slightly according to the preparation method. These nanoscale graphene materials exhibit remarkable properties, including superior stretchability, Young's modulus, thermal and electrical conductivity, and large surface area. Whether used alone or in conjunction with other nanomaterials in composites, graphene significantly enhances the performance of flexible sensors.[199] The sensor substrate itself, on which graphene is supported, consists of flexible materials including PET, PI, PDMS, stretchable elastomers, thermoplastic polyurethane (TPU), Ecoflex, textiles, paper-based substrates, and tattoo papers, Table 2. Other potential flexible materials for on-skin wearables devices, such as silk fibroin, sponge, and cellulose, have demonstrated outstanding potential. They have been recently employed due to their unique elasticity, biodegradability, and biocompatibility.[200]

The material's tensile strength is crucial for ensuring the flexibility of the sensors. Single-layer graphene has demonstrated exceptional mechanical properties, including a tensile strength of 130 GPa and a Young's modulus of 1 TPa.[211] Graphene oxide, on the other hand, has an average tensile strength of approximately 80 MPa and an average elastic modulus of about 32 GPa.[212] In addition, the electrical conductivity can affect the sensitivity. The electric conductivity of graphene is affected by its structure and size.[213] While comprehensive studies on graphene's conductivity are limited, it was reported that graphene fibres exhibit a conductivity of 2.02×10^6 S m^{-1}.[214]

Graphene can be formed into fibrous, thin-film, and three-dimensional configurations. Fibrous structures consist of nanoscale filaments, either continuous or discontinuous, created using textile processes, with diameters ranging from tens to hundreds of microns.[215] These structures are noted for their stability and excellent mechanical properties. Flexible sensors made of fibrous graphene are washable, comfortable, soft, breathable, and exhibit good electrical conductivity.[216] For thin-film flexible sensors, the electrodes resemble nanoscale thin sheets. The incorporation of microstructures on these flat, film-like surfaces, such as microdome arrays, micropyramid structures, and hollow microsphere structures, can significantly enhance their sensitivity.[217] Graphene can also be fabricated into 2D films with excellent electric and thermal properties, high flexibility, and transparency. These films are relatively easy to produce and can be scaled up, making them highly promising for commercial on-skin devices.[218] Conductive filler materials such as sponges, foams, and aerogels are used in three-dimensional sensors. The controlled porous structure and large specific surface area of these 3D materials make them highly sensitive to signal changes. The assembly

Table 2 Comparison of different substrate materials for wearable biosensor applications

Substrate	Advantages	Limitations	Ref.
PET	Lightweight, transparent, low-cost, chemically stable, compatible with roll-to-roll printing.	Poor stretchability, prone to cracking under strain, and limited conformability to skin.	201
PI	High thermal stability, chemical resistance, and excellent for high-temperature processing	Rigid and less skin-compliant, dark appearance may limit optical applications.	202
PDMS	Biocompatible, highly flexible, excellent for microfluidics and skin contact.	Hydrophobic, prone to swelling with solvents, and limited mechanical durability.	203
TPU	Stretchable, abrasion-resistant, good compatibility with skin, reusable and washable.	The surface needs functionalisation for graphene adherence.	204
Textiles	Breathable, flexible, and already integrated into daily life.	Irregular texture complicates fabrication; limited electrical uniformity.	205
Stretchable elastomers	Highly conformal with excellent stretchability, making it suitable for skin movements	Limited chemical resistance, and surface modification is often required	206
Ecoflex	Ultra-soft, highly stretchable, and has skin-like mechanical properties	Low mechanical strength and challenging in electrode patterning	207
Silk fibroin	Biodegradable, bioresorbable, highly biocompatible.	Complex processing and sensitivity to moisture.	208
Sponge-based films	Porous structure allows for high loading of analytes and improved sensitivity in 3D sensing.	Difficult to control microstructure and pattern fidelity; limited miniaturisation potential.	209
Cellulose-based films	Sustainable, biodegradable, cost-effective, and chemically modifiable.	Weak mechanical performance and instability in aqueous environments.	210

 This journal is © The Royal Society of Chemistry 2025

process for these sensors is relatively straightforward, offering significant potential for sensing applications.[219]

Graphene–skin interactions in wearable devices. Biocompatibility is critical in designing wearable biosensors, particularly for devices intended for direct and prolonged skin contact.[220] While graphene-based materials have emerged as promising components for next-generation wearable platforms, their interaction with the skin and underlying tissue remains a key safety consideration.[221]

In wearable applications, skin exposure to graphene raises concerns over potential irritation, allergic responses, or dermatitis, especially during extended use or under occlusive conditions (*e.g.*, sweat, friction, or heat accumulation).[222] While most studies suggest that graphene and its derivatives exhibit good biocompatibility, responses can vary depending on material properties such as oxidation state, surface roughness, and residual synthesis by-products.[223] For example, GO has shown dose-dependent cytotoxicity and the possibility of generating reactive oxygen species (ROS), which may pose risks in continuous-use devices.[224] In contrast, pristine graphene and LIG are often associated with low cytotoxicity, allowing good compatibility with dermal applications.[225]

More importantly, wearable-specific issues such as skin sensitivity, allergic contact reactions, or barrier function disruption have yet to be comprehensively studied for graphene-based sensors.[226] Although there are few direct allergic responses to graphene nanostructures, the lack of standardised tests for skin compatibility demands more strict dermatological testing.[227] Additionally, wearable biosensors often require encapsulation layers, carriers, or adhesives, each of which can influence the overall skin compatibility of the device.[228]

To mitigate these risks, surface functionalisation strategies using biocompatible polymers (*e.g.*, polyethylene glycol, chitosan, or polydopamine) can be applied to minimise adverse reactions and improve skin tolerance.[229] In parallel, encapsulation with breathable, hypoallergenic elastomers (*e.g.*, Ecoflex or medical-grade silicone) can help isolate active graphene layers from the skin while maintaining flexibility and performance.[230] As wearable sensors move toward continuous, 24-hour operation, ensuring dermal safety and comfort is desirable and essential for user adoption.

Sensors that utilise graphene as transducing elements should be designed with a particular property to improve their performance and detection limits.[231] Batch-to-batch variations in the synthesis process, graphene derivatives, and different synthesis methods affect the overall performance of a biosensor. Furthermore, the proper and robust orientation between graphene sheets and the biorecognition element plays a pivotal role in device sensitivity and selectivity.[232] Other parameters such as the number of graphene layers, thickness of the sheet, degree of oxidation level, and types of available surface functional groups directly influence the material's affinity towards bioreceptors, their stability over subsequent reactions, and ultimately the sensor performance.[233]

Surface chemistry modification of graphene nanostructures

Graphene has excellent and unique properties that are suitable for a wide range of applications. However, as a transducing material for biomedical applications, the surface chemistry of graphene must be tuned to conjugate with biorecognition elements. The surface modification process alters its wettability and surface charge, thereby enhancing its affinity to bioreceptors.[234] For instance, pristine graphene is insoluble, chemically inert, and non-reactive, limiting its usage for biosensing. Therefore, electron-withdrawing heteroatoms (Fig. 10b), like nitrogen, phosphorus, sulphur, or boron, are often introduced to modify their charge distribution through a process called doping.[235]

Doping is substituting or replacing carbon atoms in the lattice with other elements. Incorporating a heteroatom into

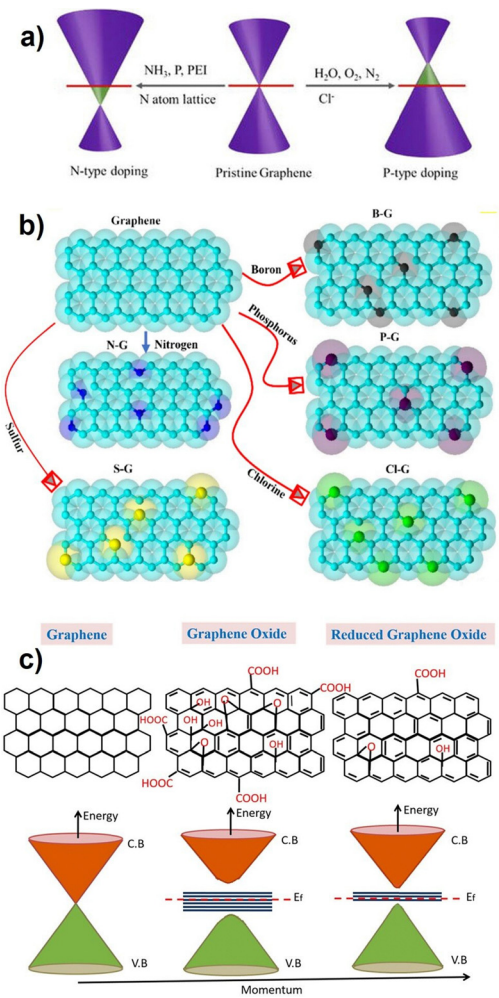


Fig. 10 (a) Doping mechanism and bandgap shifting in the graphene layer. Reprinted under terms of CC-BY 4.0 from ref. 236. Copyright © 2024, IntechOpen. (b) Schematic representation of potential placements of dopant heteroatoms within the graphene network. Reprinted with permission from ref. 237. Copyright © 2024, Elsevier. (c) Schematic representation of the lattice structure and corresponding graphene, GO, and rGO energy band diagrams. Reprinted under terms of CC-BY 4.0 from ref. 238. Copyright © 2018, Springer Nature.

the graphene lattice creates active sites that boost its reactivity since it amends the band structure, turning graphene into a semiconductor of n- or p-type, Fig. 10a.[239] Charge neutrality of graphene is compromised when a heteroatom with distinct electronegativity substitutes a carbon atom. This results in zones of unstable charges that behave as active surface sites. Consequently, structural defects may arise due to lattice strain caused by the relative size difference between the dopant and carbon atoms. This structural deformation opens the bandgap, giving it semiconducting properties and enhancing its chemical reactivity.[236] However, doping requires precise control and a relatively harsh process, and a higher level of doping is not always associated with better performance.[237] In recent studies, defect engineering has been identified as superior to doping for enhancing graphene's intrinsic reactivity by creating edge and vacancy defects. This approach produces graphene-based dopant-free catalysts with localised electrons at defect sites.[240]

Compared to pristine graphene, GO provides an abundance of oxygenated functional groups, essential for covalent coupling with biomolecules. Nevertheless, non-modified areas of the basal plane still possess a hydrophobic nature, making them prone to binding with biomolecules through π–π stacking. On the other hand, rGO retains less atomic percentage of oxygen, thereby exhibiting less hydrophilicity and dispersibility in polar solvents and possessing fewer surface charges than GOs, Fig. 10c. Consequently, GO and rGO interact differently with biomolecules, resulting in different biological responses. However, the surface functional groups of GO and rGO can still be further functionalised similarly to immobilise molecules of interest like aptamers, antibodies, proteins, DNA, drugs, MIPs, or nanoparticles.[236,238,241]

Minimal oxidation of graphene can significantly enhance the binding affinity of biomolecules. Reduced graphene oxide (rGO) possesses superior biomolecule immobilisation capability compared to GO and even pristine graphene. While pristine graphene has superior electrical properties and mechanical strength, it lacks functionalisation versatility and requires additional modification. Although GO offers abundant oxygen-containing sites needed for biofunctionalisation, poor electrical properties accompany its disrupted sp^2 hybridisation. In contrast, rGO with its partially restored sp^2 network strikes a perfect balance between electrical properties and availability of oxygen moieties, making it exclusively stable, sensitive, and suitable for biosensing applications.[242,243] For example, Yu *et al.* showed that the level of GO oxidation negatively influences the fluorescence-quenching properties and immobilisation efficiency of single-stranded DNA (ssDNA) aptamers.[242] The team confirmed the importance of minimal oxidation of graphene for the enhanced binding affinity of ssDNA, highlighting the role of decreased oxygen content, particularly in rGO, in improving DNA-sensing efficiency.

Further functionalisation of graphene surfaces is crucial to tailor the material for a specific purpose. This process affects the hydrophobicity and surface charge of the material, and can take place either through covalent or non-covalent interactions.

Covalent functionalisation. Covalent interactions are responsible for forming strong bonds between the available functional groups on the graphene surface and the bioreceptor through irreversible chemical interactions. Covalent coupling can be achieved with various chemical processes such as condensation, cycloaddition, electrophilic, and nucleophilic reactions. This process generally comes at the cost of altering the electrical and mechanical qualities of graphene, as that bond results in a localised change in graphene hybridisation from sp^2 into sp^3 bond. However, covalent coupling boosts its solubility, widens the bandgap, strengthens the stability and structural robustness, and enhances its affinity to biorecognition elements. The most used forms of graphene in covalent coupling are GO and rGO, owing to the availability of carboxyl (–COOH) and hydroxyl (–OH) groups on their surface, which are usually involved in the cross-linking reactions.[236]

The key function of cross-linkers is establishing a strong bond between the thiol, amine, or carboxylic acid group on biomolecules and functional groups on the graphene surface. As illustrated in Fig. 11a, establishing a bond between GO/rGO and a $-NH_2$-containing bioreceptor requires activation of carboxylic groups into o-acylisourea intermediate, a reactive, unstable ester.[127] Several cross-linkers can be used to activate carboxyl groups, including 1-ethyl-3-(3-dimethyl aminopropyl) carbodiimide (EDC), *N*,*N*-dicyclohexyl carbodiimide (DCC), thionyl chloride ($SOCl_2$), and 2-(7-aza-1*H*-benzotriazole-1-yl)-1,1,3,3-tetramethyluronium hexafluorophosphate, which enable adequate covalent coupling.[244]

In most cases of antibody or protein coupling, the reactive ester is produced by EDC coupling, before which it is paired with *N*-hydroxysuccinimide (NHS), or its water-soluble form (Sulfo-NHS), to establish a stable ester that withstands physiological pH. Subsequently, such esters can establish a stable and strong amide bond with biomolecules by reacting with the primary amines. The EDC/NHS crosslinking chemistry, shown in Fig. 11b, was used in a wearable biosensor to bind cortisol monoclonal antibodies onto the surface of LIG, achieving elevated sensitivity to cortisol levels in sweat.[63] This biomolecule immobilisation strategy is the most common tool for covalent functionalisation in wearable technologies.

Glutaraldehyde (GA) cross-linking has also been reported for anchoring enzymes, such as glucose oxidase (GO_x), to rGO surfaces. This approach links oxygen moieties on the pretreated rGO surface with amine groups of GO_x to achieve a stable covalent bond.[246] Silanisation is another efficient method for inducing functional groups on graphene surfaces. Some silanes can bind covalently and grow SAMs with oxygen-containing graphenes facilitated by their methoxy groups. Silicon (Si) in silanes binds to the hydrolysed surface of graphene through the –OH groups. The remaining free Si–X bonds are then hydrolysed, allowing for the formation of strong Si–O–Si linkages between silane layers (Fig. 11c),[127] establishing a monolayer of silanols (SiOH).[247] The most commonly used silanes in biosensing, including 3-aminopropyltrimethoxysilane (APTES), (3-mercaptopropyl)trimethoxysilane (MPTMS), 3-glycidoxypropyltrimethoxysilane (GPMS), and 3-glycidoxypropyldimethylethoxysilane

 This journal is © The Royal Society of Chemistry 2025

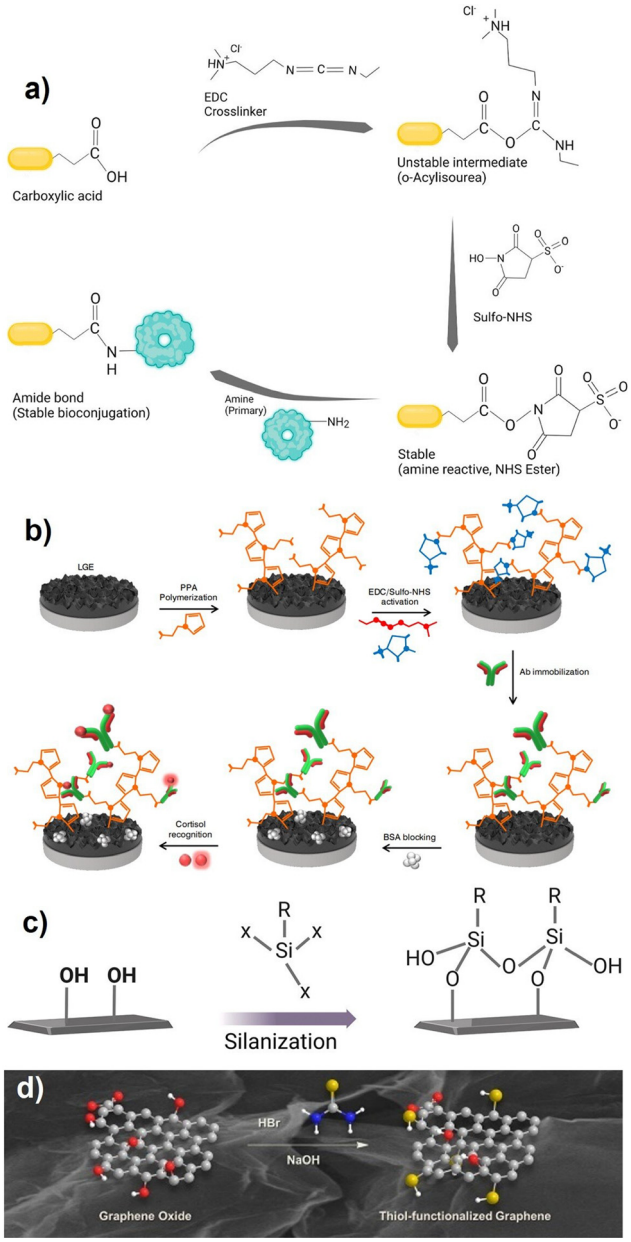


Fig. 11 (a) Chemical reaction scheme of EDC/(sulfo)-NHS coupling, illustrating the activation of a carboxyl group on the electrode surface to form a stable amine-reactive NHS ester, followed by covalent attachment of a primary amine from the bioreceptor. Reprinted under terms of CC-BY 4.0 from ref. 127. Copyright © 2023, Elsevier. (b) Schematic representation of the modification procedure for the graphene electrode used in cortisol sensing. Reprinted with permission from ref. 63. Copyright © 2020, Elsevier. (c) Schematic depiction of silanisation formation on hydroxylated substrates. Reprinted under terms of CC-BY 4.0 from ref. 127. Copyright © 2023, Elsevier. (d) Functionalisation of GO with a thiol group to provide a thiolated graphene lattice. Reprinted with permission from ref. 245. Copyright © 2015, American Chemical Society.

(GPMES), can bind and grow into SAMs onto graphene substrates. Upon binding of silanes, the other exposed terminal usually carries the desired functional groups, including thiol, amine, and carboxylic groups, needed for bioconjugation.[127]

Aside from silanisation, certain dopants can also introduce new functional groups into the graphene lattice. For instance, thiol (–SH) functionalisation is a widely used strategy for modifying graphene electrodes to enhance their reactivity with biomolecules. Thiol groups are known for their strong affinity to gold and ability to bind covalently to graphene or graphene derivatives. One example is introducing a single type of sulphur moiety (monothiolation) to GO suspensions through thiourea, a thiol-containing compound. This method showed great potential for simultaneous functionalisation and partial reduction of GO into thiol-functionalised rGO, Fig. 11d. Chemical doping increases the electrode's reactivity towards biomolecules and enhances their electrical conductivity as well.[245,248]

Non-covalent functionalisation. Non-covalent interactions mostly depend on achieving a relatively stable dispersion through weak stabilising mechanisms. The physical adsorption or adhesion of molecules on the graphene surface could be established through weak interactions such as hydrophobic interaction, π–π stacking, electrostatic interaction, hydrogen bonding, and van der Waals forces.[249] Despite the more substantial and irreversible linkages achieved by covalent coupling, non-covalent bonding shows superiority in preserving sp^2 configuration and electrical properties of graphene, as well as retaining a substantially sizeable active surface area.[250] Self-assembled monolayer (SAM) technique is one of the approaches to introducing functional groups to the bare graphene surface. SAMs are ultrathin and highly organised layers formed by the adsorption and subsequent uniform growth of organic compounds onto the graphene surface.[251] These highly ordered monolayers possess a head group that usually interacts with the substrate, whereas the tail group is modified with the desired functional groups for further functionalisation with biomolecules.[252]

One of the most stable and widely used SAM-based modification strategies is AuNPs–thiol SAM crosslinking. This process starts by depositing AuNPs by reducing the tetrachloroaurate ($AuCl_4^-$) precursor, producing p-type doping effects. Next, thiol-SAM organic compounds terminating in an –SH group interact favourably with the gold surface, producing n-type doping effects and thereby controlling the Fermi level of graphene.[253] Fig. 12a illustrates the self-assembly of –SH terminated organic compounds on AuNP-doped surfaces, facilitating the immobilisation of biomolecules onto the other carboxyl/amine-containing terminal. A stable monolayer of SAM requires a two-step process. The first step is fast, involving the physical adsorption of SAMs on the surface. The second step is slower, ensuring reordering of the monolayer conformation and converting physisorption into stronger chemisorption.[127] This surface modification strategy exploits and anchors heavy metal ions to control the Dirac voltage, Fig. 12b.[254]

Silanisation is another efficient method of inducing functional groups onto the graphene surface. Silanisation is considered non-covalent, because silanes interact non-covalently with graphene to form SAMs.[257] For instance, amino-silanes,

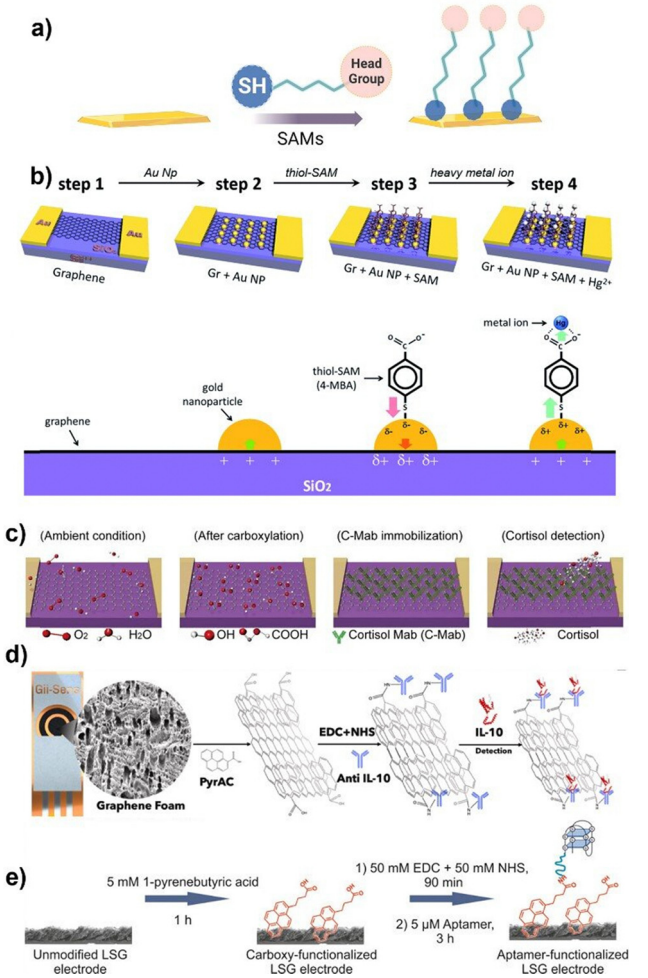


Fig. 12 (a) Schematic representation of the formation of SAMs. Reprinted under terms of CC-BY 4.0 from ref. 127. Copyright © 2023, Elsevier. (b) Fabrication process of a graphene FET device with enlarged views showing configurations and charge transfer directions: gold nanoparticle deposition induces partial p-type doping on graphene (step 2); thiol-SAM molecules (4-mercapto benzoic acid, 4-MBA) induce n-type doping (step 3); and heavy metal ion capture induces p-type doping (step 4). Reprinted under terms of CC-BY 3.0 from ref. 254. Copyright © 2021, Elsevier. (c) UV-ozone-mediated cortisol monoclonal antibody (Cortisol-mAb) immobilisation. Reprinted under terms of CC-BY-NC 4.0 from ref. 255. Copyright © 2020, The American Association for the Advancement of Science. (d) Printed microfluidic system and SEM image of the Gii-sense graphene foam, including a scheme of the surface chemistry modification with PCA and subsequent immobilisation of anti-IL-10 antibodies. Reprinted with permission from ref. 256. Copyright © 2023, Elsevier. (e) Functionalisation process of LIG electrodes by PBA followed by EDC/NH to finally immobilise aptamers. Reprinted with permission from ref. 123. Copyright © 2017, American Chemical Society.

such as APTES, are used to induce amine ($-NH_2$) groups on graphene surfaces through π–π interactions or hydrophobic interactions with graphene, exposing amine groups at the other end for coupling with AuNPs. Subsequently, AuNPs can be readily crosslinked with EDC/NHS or conjugated with other functional groups for biosensing applications. For example, a graphene-modified glassy carbon electrode was silanised by APTES to generate amine groups that would subsequently be used for coupling AuNPs. Thiolated DNA aptamers were then crosslinked with the functionalised graphene surface to develop a biosensor for thrombin.[258]

Silanes can also be used to introduce functional groups for various applications. Graphene is treated with silane coupling agents to induce –SH groups onto the surface, facilitating its reaction with gold nanoparticles.[259] The thiol-silanes, including MPTMS, can non-covalently interact with bare pristine graphene surfaces by physical adsorption. The other exposed thiol-containing terminals then anchor gold nanoparticles, creating a strong S–Au bond. Therefore, thiolated biomolecules such as aptamers and antibodies can be conjugated with the AuNPs directly using thiol chemistry.[260]

Oxygen moieties can be introduced onto graphene surfaces through carboxylation by exposure to ultraviolet ozone (UVO) for one or two minutes. This process generates superficial oxygen moieties and enhances surface wettability. Functionalised surfaces can then be used for the conventional EDC/NHS covalent coupling with the amine-containing probe, Fig. 12d. However, prolonged UVO exposure leads to undesired electrical and physical properties. This method has been used in G-FET-based smart contact lenses to immobilise cortisol antibodies.[255] Additionally, the graphene lattice can be modified with the central macrocycle of tetrakis(4-carboxyphenyl) porphyrin (TCPP) *via* a physical π–π stacking, inducing oxygen-containing functional groups (carboxyphenyl) on the surface. Subsequently, EDC/NHS crosslinking can both activate the generated groups and link amine-containing probes. Zhang *et al.* used this approach to immobilise aptamers on the graphene surface for cortisol detection.[149]

A common non-covalent approach for modifying the graphene surface involves aromatic molecules, specifically pyrene derivatives, which interact through π–π stacking with the sp^2-hybridised lattice of graphene. Upon adsorption to the surface, the terminal carrying the desired functional groups, such as amine ($-NH_2$) or carboxyl (–COOH) groups, is exposed and can be further utilised for immobilising biomolecules such as antibodies or aptamers.[261] For instance, the surface chemistry of flexible graphene-foam electrodes was non-covalently modified using π–π interactions between pyrene carboxylic acid (PCA) and graphene.[256] This modification preserves the electrical properties of graphene while enhancing the wettability of the electrode.

Another commonly used pyrene derivative for introducing oxygenated functional groups is the 1-pyrenebutyric acid (PBA). Balaban *et al.* demonstrated anchoring PBA on bare graphene electrodes and subsequent activation of the induced groups *via* EDC/NHS cross-linking.[262] Fenzl *et al.* used PBA to functionalise laser-induced graphene to covalently bind antibodies.[263] Similarly, the same crosslinker was used to functionalise the LIG surface to generate carboxylic groups required for subsequent modification with aptamers by EDC/NHS covalent coupling. The anchoring process was efficiently done by π–π stacking and hydrophobic interactions, Fig. 12e.

Functionalisation can also take place by 1-pyrenebutyric acid *N*-hydroxysuccinimide ester (PBSE), which possesses a

 This journal is © The Royal Society of Chemistry 2025

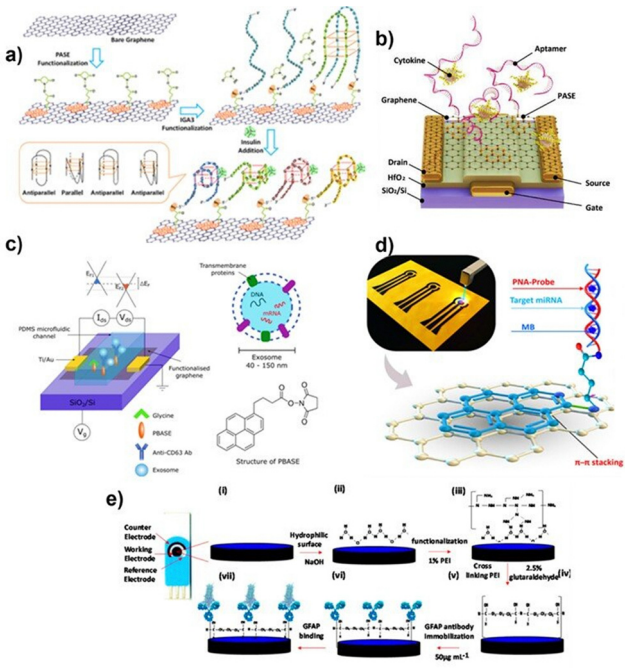


Fig. 13 (a) The graphene nanosensor for insulin detection is prepared *via* a Schiff-base reaction between aptamer IGA3 and a graphene-immobilised PASE linker. Insulin binding induces the formation of parallel and antiparallel G-quadruplexes, bringing negatively charged insulin and DNA strands close to the graphene surface, disrupting carrier concentration and generating detectable signals. Reprinted with permission from ref. 265. Copyright © 2017, American Chemical Society. (b) An aptameric GFET with a buried-gate geometry is used for cytokine detection. Reprinted with permission from ref. 266 Copyright © 2019, Elsevier. (c) The functionalised biosensor with microfluidic integration shows doping differences in covered and uncovered graphene due to exosome binding, illustrated by the basic structure of an exosome and the molecular structure of (PBASE). Reprinted under terms of CC-BY 4.0 from ref. 267. Copyright © 2019, Springer Nature. (d) A proposed PNA-functionalized LIG biosensor involves a single-step functionalisation process based on π–π stacking between pyrene-modified PNA probes and graphene. Reprinted under terms of CC-BY 4.0 from ref. 268. Copyright © 2024, American Chemical Society. (e) The surface modification stages for GFAP antibody immobilisation on graphene electrodes involve multiple steps: (i) creating a hydrophilic surface *via* sodium hydroxide (NaOH) treatment, (ii) functionalisation with polyethylenimine (PEI), (iii) surface activation using glutaraldehyde, (iv) Schiff-base formation, (v) immobilisation of the GFAP antibody, (vi) blocking unbound sites, and (vii) final preparation of the immunosensor for detection. Reprinted with permission from ref. 269. Copyright © 2018, American Chemical Society.

pyrene group that binds physically with graphene and an ester group that interacts with amine groups. Accordingly, PBSE can form amide bonds between primary amines in bioreceptors and the exposed ester groups without EDC/NHS crosslinking.[264] This technique was used to develop an aptameric G-FET sensor for monitoring insulin levels indirectly through IGA3 isoforms, a subclass of immunoglobulin A (IgA) antibodies. Such antibodies are targeted by guanine-rich insulin-specific IGA3 aptamers, previously linked with PBSE, Fig. 13a.[265] The same team later utilised this technique to attach the IL-6 aptamer on the graphene surface to detect the level of IL-6 cytokine in saliva, Fig. 13b.[266] Tsang *et al.* employed the same technique to immobilise anti-CD63 antibodies for exosome detection, Fig. 13c.[267]

Khan *et al.* recently introduced a new technique that allows chemical modification of the biological probe with the crosslinker beforehand to promote robust coupling with graphene, simplifying the immobilisation process.[270] For instance, Barman *et al.* used this method for a single-step functionalisation of LIG *via* PBSE for smartphone-based detection of *has*-miR-141, a prostate cancer biomarker.[268] The team synthesised an integrated π–π stackable bespoke 1-pyrenebutyryl-N-end-terminated peptide nucleic acid (Py-PNA) before immobilising it into the bare graphene surface, Fig. 13d. The synthesis of a complementary strand started with solid-phase peptide synthesis of a 17-mer probe, followed by adding two positively charged arginine amino acid residues to its N-terminus to enhance the probe's solubility. Finally, the PBSE was used to modify the N-terminus to facilitate a single-step π–π stacking on graphene. The pre-functionalisation step showed enhanced stability and uniformity on the graphene surface, making it ideal for sensitive and reliable biosensing applications.

The presence of amine groups (–NH_2) is critical for efficient functionalisation. One practical method for introducing –NH_2 groups on bare graphene electrodes is the deposition of polyethyleneimine (PEI).[271] A study has reported the prior treatment of the hydrophobic surface of graphene screen-printed electrodes with 1 M sodium hydroxide (NaOH) to generate oxygenated functional groups and render the hydrophilicity of the electrode. Subsequently, the electrode is functionalised with 1% PEI to introduce –NH_2 groups needed for anchoring antibodies. Facile antibody conjugation then took place by crosslinking with 2.5% GA to detect glial fibrillary acidic protein (GFAP), which is associated with central nervous system (CNS) injuries, Fig. 13e.[269]

Blocking adsorption active sites on the graphene surface is a means for improving sensing accuracy. This approach avoids non-specific binding with a minimal loss of inherent qualities and structure of the material.[272] The blocking process can be carried out by non-covalent interaction of coating agents, such as bovine serum albumin (BSA), ethanolamine, superblock, and casein, or by surface treatment with surfactants such as Tween.[273]

Research on graphene-based biosensors

Analysing body fluids provides a non-invasive method for assessing physiological conditions. Various substances, including glucose, metal ions, cortisol, and lactic acid, can be evaluated with this sample.[274] Given its substantial specific surface area, graphene serves as an excellent platform for surface modification, allowing for the detection of numerous chemical signals based on the chosen modifier. Graphene chemical sensors typically employ two primary device architectures: the three-electrode system and the FET structure.[275]

Graphene serves as the working electrode (WE) in the three-electrode electrochemical setup. Platinum or other carbon-based materials act as the counter electrode (CE) to ensure adequate current flow to the WE. A silver/silver chloride (Ag/

AgCl) electrode serves as the reference electrode (RE), offering a stable reference potential.[276] Conversely, graphene is utilised as the channel material in the FET structure and modified with specific biorecognition elements. When these elements interact with target analytes, they alter the carrier density within the channel, consequently affecting the transfer and transmission characteristics of the graphene FET (G-FET).[277]

Graphene-based electrochemical biosensors. Electrochemistry-based transducers are the most reliable and flexible options for designing wearable sensors due to their sensitivity, ease of fabrication, absence of moving parts, mechanical robustness, and resistance to varying conditions. This transducing concept remains the most widely used and trusted option for biosensors.[278]

Sharma *et al.* developed a LIG-based pH sensor for urea detection. The sensor is flexible and compatible with catheters. The sensor successfully detected urea concentrations as low as 10^{-4} M, with a response time of less than 1 minute. The electrostatic and covalent immobilisation of chitosan on LIG can increase the amount of immobilised urease. Urease catalyses the hydrolysis of urea into CO_2 and ammonia, which can be easily detected with the LIG-based pH sensor. The hydroxyl and amino groups present in chitosan enable both electrostatic and covalent immobilisation strategies and, hence, increase the quantity of the immobilised enzyme.[279] Hui *et al.* reported LIG/PDMS electrodes functionalised with platinum and AuNPs for detecting dopamine (DA) in a standard solution and human urine, showing acceptable selectivity for interfering substances such as UA and ascorbic acid (AA).[280]

Wan *et al.* reported a LIG-based biosensor for the detection of preeclampsia-specific miRNA.[281] The authors demonstrated that nitrogen (N) atoms in the precursor PI were partially incorporated into the LIG in the form of pyrrolic N (1.6 to 4.4%) and graphitic N (from 2.4 to 4.5%). The self-N-doped porous LIG possesses enhanced conductivity as an electrochemical sensor and improved sensitivity to nucleic acids. This study suggested that the self-N-doped LIG has great potential as a simple and low-cost biosensing platform for detecting and analysing nucleic acids.

Barman *et al.* reported an electrochemical immunosensor using cationic polyelectrolyte polyallylamine (PAAMI)–anchored LAG as the electrode. The addition of the PAAMI provided abundant clipping sites for fixing antibodies by introducing the amino group. Electrostatic adsorption increases the stability of the LAG flakes. Electrodeposition decorates PAAMI@LAG with Pt nanoparticles, which offers a fast electron transfer rate. The immunosensor detected IgG as a proof of concept.[282] Yang *et al.* demonstrated an entirely laser-engraved graphene-based sensor (Fig. 14a–f) for simultaneous sweat sampling, chemical sensing, and vital sign monitoring.[283] The physical sensor continuously detects temperature and respiration rate, while the chemical sensor monitors low concentrations of UA and tyrosine (Tyr) analytes associated with gout and metabolic disorders.

Beduk *et al.* reported an electrochemical immunosensor based on LSG decorated with 3D gold nanostructures for the diagnosis of coronavirus (COVID-19).[284] Following a proper surface modification step, this electrode was functionalised with antibodies to the SARS-CoV-2 spike (S) antigen. This LSG-based electrochemical immunosensor can offer faster readout time compared to commercial diagnostic tools and provide a promising alternative method for affordable and rapid PoC devices.

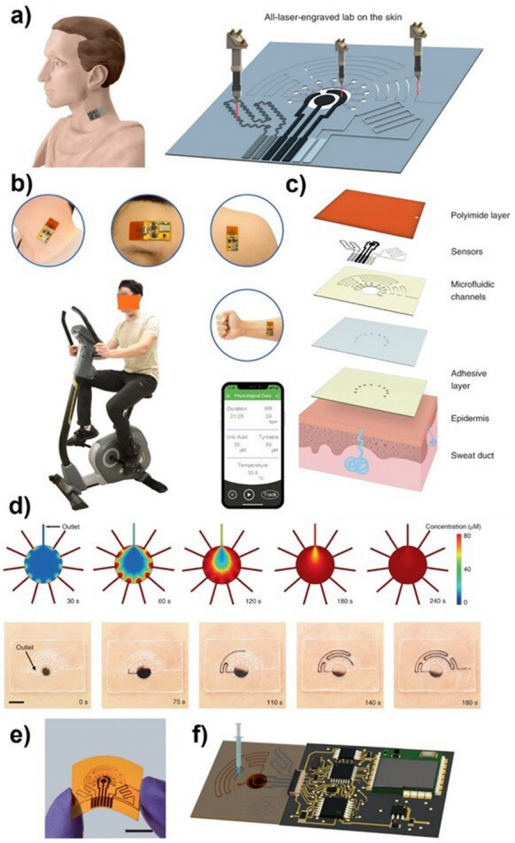


Fig. 14 (a) The sensor comprises entirely laser-engraved components, including the microfluidic module and LEG-based chemical and physical sensors. (b) Photographs show a healthy subject wearing the sensor patch on different body parts. (c) Layers of the sensor are shown, ranging from the bottom layer in contact with the epidermis to the top layer. The sensor performs multiple functions, such as ultrasensitive sweat UA and Tyr detection, sweat rate estimation, temperature sensing, and vital sign monitoring (*e.g.*, heart rate and respiration rate). (d) Simulations illustrate solute concentration distributions over the bottom surface of the reservoir at various time points (inlet flow rate: 1.5 μL min^{-1}). Photographic images depict microfluidic sweat sampling during an iontophoresis-induced sweat secretion process (scale bar: 5 mm). (e) A photographic image of the flexible lab-on-skin patch is shown (scale bar: 1 cm). (f) The flow test setup demonstrates wireless monitoring of analyte levels, with a syringe pump injecting analyte solution through an inlet. Reprinted with permission from ref. 7. Copyright © 2019, Springer Nature.

Torrente-Rodríguez *et al.* proposed a highly sensitive, selective, miniaturised device (Fig. 15a and b), based on a laser-enabled flexible graphene sensor for non-invasive monitoring of the level of stress hormones.[63] Antibody functionalisation of the electrode surface was carried out with electropolymerisation of 1H-pyrrole propionic acid (PPA). This process improves the strength and adhesion of polymeric films to the transducer

 This journal is © The Royal Society of Chemistry 2025

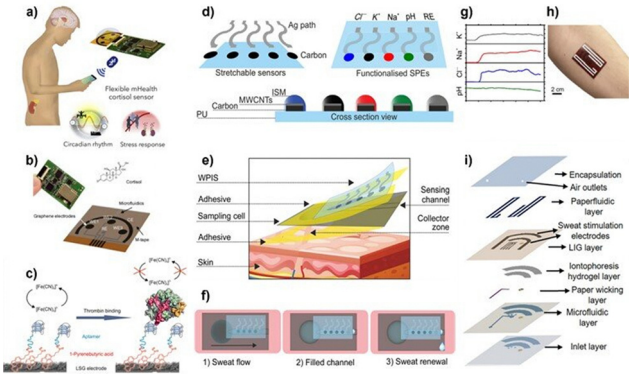


Fig. 15 (a) Schematic representation of the flexible cortisol sensor. (b) Design of the flexible microfluidic three-working-electrode sensor array for cortisol detection, along with a photograph of the printed circuit board with the graphene sensor patch for signal processing and wireless communication. WE: working electrode; CE: counter electrode; RE: reference electrode. Reprinted with permission from ref. 63. Copyright © 2020, Elsevier. (c) Schematic illustration of the thrombin electrochemical detection mechanism shows that increasing thrombin concentrations hinder the diffusion of the redox marker hexacyanoferrate(III) to the electrode surface, thereby decreasing peak currents in voltammetric measurements. Reprinted with permission from ref. 123. Copyright © 2017, American Chemical Society. (d) Comparison of electrodes before and after functionalisation. (e) WPISs (wearable potentiometric ion-selective sensors) are attached to the skin, whereas ISM refers to the ion-selective membrane. (f) Sweat flows in the sampling cell after attachment to the skin. (g) Concentration profiles were recorded with WPISs during a 60-minute cycling workout. Reprinted under terms of CC-BY-NC 4.0 from ref. 285. Copyright © 2019, American Chemical Society. (h) Optical image of a wearable device placed on the forearm of a human subject. (i) A stacked view of the wearable device showcases the various functional layers and components. Reprinted under terms of CC-BY 4.0 from ref. 286. Copyright © 2024, American Chemical Society.

surface and facilitates subsequent surface modifications with carboxylate moieties for affinity-based sensor fabrication. The team reported a strong correlation between sweat and circulating cortisol and demonstrated the prompt change of sweat cortisol in response to acute stress stimuli.

Fenzl *et al.* demonstrated a reliable and sensitive LIG biosensor functionalised with aptamers to detect thrombin in serum.[263] The LIG electrodes were created in a PI film. A universal immobilisation approach is established by anchoring 1-pyrenebutyric acid to the LIG and subsequently covalently attaching an aptamer against the thrombi as a specific bioreceptor to the carboxyl groups, Fig. 15c.

Garg *et al.* recently reported the unique integration of LIG electrodes with paper microfluidics to monitor cortisol levels in sweat with MIPs as bioreceptors.[286] The device was equipped with an iontophoretic system of two arc-shaped LIG electrodes to induce sweat secretion on demand. The device operates *via* label-free EIS and shows an exemplary specificity and sensitivity not only to cortisol but also to sodium ion concentration and sweat dynamics, Fig. 15h and i. Xu *et al.* fabricated a highly selective electrochemical sensor based on a PEDOT-modified LIG for detecting dopamine (DA) in the presence of AA and UA.[287] LSG electrodes were created with a 3D macro-porous network and large electrochemically active surface area *via* direct laser writing on polyimide sheets. PEDOT was electrodeposited on the LSG electrode. Zhu *et al.* utilised uniform electroless plating of nickel and gold layers on porous LIG electrodes to significantly enhance sensitivity and the linear range of glucose sensing.[288] In addition to the reduced requirement for the fundamental solution, this work integrates a porous encapsulating reaction cavity containing alkali solutions with a soft, skin-interfaced microfluidic component to provide integrated microfluidic non-enzymatic glucose sensors for sweat sampling and glucose sensing.

Lei *et al.* derived a new patterning process for highly conductive nitrogen-doped graphene from a lignin-based precursor.[289] CO_2 laser produced porous graphene electrodes from lignin under ambient air conditions. The resulting nitrogen-doped LIG (N-LIG) is binder-free, hierarchical, and conductive. The interconnected carbon network displayed enhanced electrochemical activity with an improved heterogeneous electron transfer rate. These features can be attributed to the high conductivity of porous N-LIG (down to 2.8 Ω per square) and its enriched active edge-plane sites. Furthermore, the N-LIG electrodes were decorated with an MXene/Prussian blue ($Ti_3C_2T_x$/PB) composite *via* a simple spray-coating process. The $Ti_3C_2T_x$/PB-modified N-LIG electrodes were functionalised with catalytic enzymes for detecting glucose, lactate, and alcohol. These electrodes exhibited remarkably enhanced electrochemical activity toward biomarkers with a performance on par with previously reported on-chip carbon-based biosensors.

Wang *et al.* reported a wearable electrochemical biosensor for continuously analysing trace levels of multiple metabolites and nutrients in sweat during physical exercise and at rest, including all essential amino acids and vitamins.[290] The biosensor consists of graphene electrodes that can be repeatedly regenerated *in situ*, functionalised with metabolite-specific antibody-like molecularly imprinted polymers (MIPs) and redox-active reporter nanoparticles, and integrated with modules for iontophoresis-based sweat induction, microfluidic sweat sampling, signal processing and calibration, and wireless communication.

Tu *et al.* reported a wearable and wireless patch for the real-time electrochemical detection of the inflammatory biomarker CRP protein in sweat.[291] The device integrates iontophoretic sweat extraction, microfluidic channels for sweat sampling and reagent routing and replacement, and a graphene-based sensor array for quantifying CRP (*via* an electrode functionalised with anti-CRP capture antibodies-conjugated gold nanoparticles), ionic strength, pH, and temperature sensors. AuNPs conjugated with electroactive redox molecule thionine (TH) and detector antibody (dAb) enabled efficient electrochemical signal transduction (signal ON) and further signal amplification. The integrated graphene sensors for measuring pH, temperature, and ionic strength enable real-time, personalised CRP data calibration to mitigate the interpersonal sample matrix variation-induced sensing errors and provide a more comprehensive assessment of the inflammatory status.

Some flexible PoC devices hold great potential for further adaptation to a wearable setting. Soares *et al.* developed a LIG-based electrochemical immunosensor to detect *Salmonella typhimurium*. The LIG electrodes were fabricated on a polyimide film under ambient conditions.[292] Following functionalisation with *Salmonella* antibodies, the LIG biosensors could detect live *Salmonella* in chicken broth. Recently, Barman *et al.* reported a peptide nucleic acid (PNA)-functionalised LIG biosensor tailored for detecting prostate cancer biomarkers (hsa-miR-141).[293] The surface chemistry employs a facile single-step functionalisation strategy through π–π stacking. The device showed high specificity towards the target analyte with a detection limit of 0.6 aM, making it a potential candidate for implementation in wearable technologies.

Reduced graphene oxide (rGO) has emerged as a viable candidate for wearable sensors due to its ease of incorporation of functional groups and ease of synthesis. Xuan *et al.* used rGO to construct an on-skin device for glucose sensing in sweat.[294] The fabrication process started with the hydrothermal reduction of GO to yield a high-quality rGO, which was then deposited onto the flexible PI substrate by spray coating. The surface was then decorated with gold-platinum alloy nanoparticles (Au-PtNPs) *via* electrochemical deposition, forming a stable nanostructured composite. Next, chitosan–glucose oxidase composites were bound with the functionalised rGO-composite surface to create a functional amperometric glucose biosensor.[254] Shu *et al.* reported the synthesis of stretchable nickel–cobalt (Ni–Co)-based metal–organic framework (MOF)/silver/reduced graphene oxide/polyurethane (Ni–Co-MOF/Ag/rGO/PU) composite fibre as the building unit for wearable devices.[295] The device was developed for non-invasive glucose monitoring in human sweat. The composite showed excellent stability under physical stress and can be incorporated into stretchable fabrics for continuous glucose monitoring. Chen *et al.* developed a novel modification method for LIG by integrating rGO on the electrode surface for the detection of breast cancer-associated exosomes.[296] Combining both materials improved the electrical conductivity of the electrode. Furthermore, hydrophobicity and reactivity with biomolecules significantly increased, facilitating efficient antibody immobilisation.

Carbon nanotubes have been intensively applied in biosensor research owing to their excellent properties. Parrilla *et al.* reported MWCNT-based wearable potentiometric ion sensors (WPISs) for continuous measurement of sweat parameters during exercise.[285] The WPIS provides complete dynamic sweat profiles, including pH value and concentration of ions (Na^+, K^+, and Cl^-), with high accuracy and minimal drift, Fig. 15d–g. Jeerapan *et al.* reported a CNT-based biofuel cell (BFC) integrated with textiles.[297] Both CNT ink and silver nano ink were screen-printed in serpentine designs on textile substrates like socks. The printed material is highly durable against mechanical deformations, in addition to acting as a self-powered sensor that can inspect and provide signals on sweat-rich biomarkers such as glucose and lactate. These energy-harvesting technologies allow for developing reliable, self-powered wearable electronics.

Graphene transistor-based biosensors. A flexible F-G-FET biosensor is an emerging and promising technology for real-time monitoring of biomarkers and other disease-associated parameters. These sensors proved to be utterly reliable when working in a wearable setting owing to their durability and tensile strength. For instance, Kwon *et al.* initially proposed that conducting polymers containing heteroatoms could be utilised to prepare doped graphene.[298] The team successfully synthesised nitrogen-doped, few-layer graphene from polypyrrole (PPy-NDFLG). They incorporated the PPy-NDFLG with RNA aptamers specific to vascular endothelial growth factor (VEGF) onto a flexible FET platform based on a polyethylene naphthalate (PEN). This study was the first to employ nitrogen-doped graphene to produce a flexible FET-based aptamer sensor for detecting VEGF as a cancer biomarker, achieving a detection limit of 100 fM. Cheng *et al.* prepared a PDMS-supported G-FET gated in PBS with an Ag/AgCl reference electrode solution.[299] The flexible PDMS substrate was modified with APTES to form an amino-group-ended surface. Graphene nanosheets were then self-assembled by covalent bonding with the terminal amino group on the PDMS surface. The device was subsequently utilised for label-free identification of the tumour marker alpha-fetoprotein (AFP), with a sensitivity threshold extending to 300 ng mL^{-1}.

Farid *et al.* fabricated a G-FET sensor also on PDMS substrates to detect interferon-gamma (IFN-γ), a biomarker for pneumonia and cancer.[300] The sensor employed a DNA aptamer probe to achieve precise and specific detection. The flexible sensor demonstrated remarkable sensitivity, enabling the detection of IFN-γ protein across a wide concentration range from nanomolar to micromolar levels. Yang *et al.* developed a G-FET sensor (Fig. 16a), with a sensing element comprising a graphene nanomesh (GNM) featuring 3 nm pores. The GNM is a continuous two-dimensional graphene nanostructure with a high density of holes punched in the basal plane, introducing lateral confinement and improving the on/off ratio. The graphene carrier concentration and mobility can be adjusted to enhance the sensing performance. Functionalising the G-FET with an aptamer allowed for the detection of human epidermal growth factor receptor 2 (HER2) with a minimum detectable level of 0.6 pM.[301]

Hao *et al.* reported another G-FET device (Fig. 16b and c), which incorporates unique DNA aptamers that are specific to tumour necrosis factor-alpha (TNF-α).[306] Aptamers were immobilised on a graphene-thin film attached to a 125-μm-thick PEN substrate. This work demonstrated that the sensor could specifically respond to changes in TNF-α concentration within 5 min and an ultra-low detection capability of 26 pM in a repeatable manner. Wang *et al.* fabricated a flexible and stretchable G-FET sensor on a 2.5-μm thick Mylar substrate to detect TNF-α.[302] The sensor possesses a high degree of flexibility and can conform to non-planar surfaces such as human skin or curved contact lenses. The device showed high selectivity and specificity towards the target analyte. The same group developed a G-FET biosensor composed of a graphene–Nafion composite.[303] The graphene–Nafion composite film minimises

 This journal is © The Royal Society of Chemistry 2025

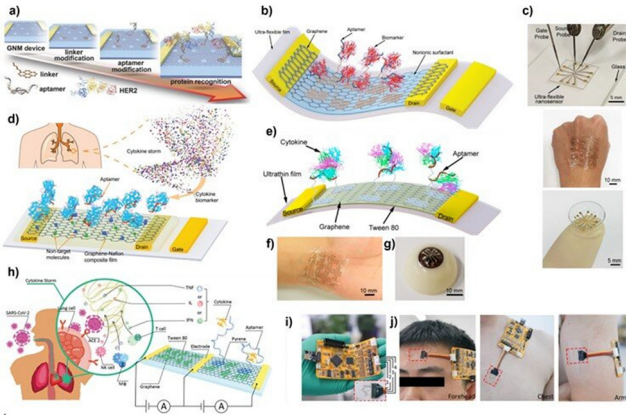


Fig. 16 (a) Schematic illustration of the fabrication process of the GNM FET biosensor. Reprinted with permission from ref. 301. Copyright © 2016, John Wiley and Sons. (b) Schematic of the ultraflexible aptameric G-FET nanosensor. (c) A photograph of the nanosensor placed on a glass slide for biomarker detection (top), mounted conformably on a human hand (centre), and a contact lens (bottom). Reprinted with permission from ref. 302. Copyright © 2019, John Wiley and Sons. (d) Schematic of the aptameric graphene–Nafion FET biosensor for cytokine biomarker detection. Reprinted with permission from ref. 303. Copyright © 2020, John Wiley and Sons. (e) Schematic of the ultra-flexible G-FET biosensor. (f) Photograph of the flexible G-FET device attached to a human wrist. (g) Photograph of the F-ET device mounted on an artificial eyeball. Reprinted under terms of CC-BY 4.0 from ref. 304. Copyright © 2020, MDPI. (h) Schematic representation of the aptameric biosensor for detecting cytokine storm syndrome biomarkers caused by COVID-19. (i) Photograph of a flexible aptameric biosensor device. (j) Fully integrated device designed for comfortable wear on different body parts, such as the forehead, chest, and arm. Reprinted with permission from ref. 305. Copyright © 2021, John Wiley and Sons.

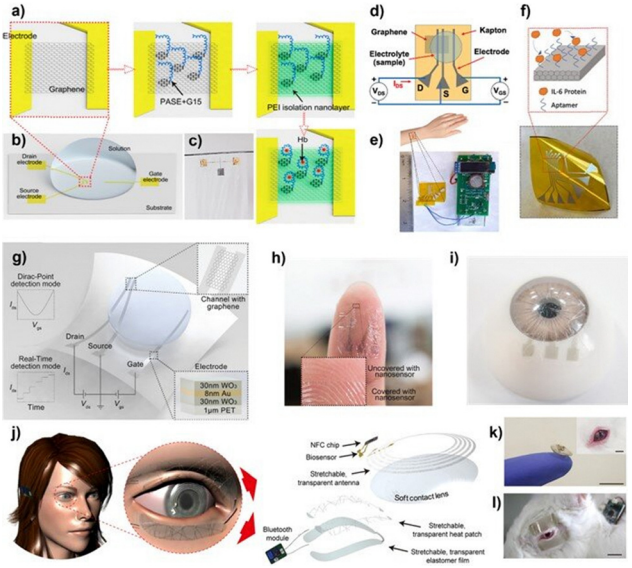


Fig. 17 (a) Schematic representation of the biochemical functionalisation steps for the G-FET-based aptameric nanobiosensor for hemoglobin (Hb) detection. (b) Illustration of the PEI-modified GFET-based aptameric nanobiosensor. (c) Photograph of the ultrathin, flexible aptameric nanobiosensor folded around a metal needle (radius: 0.5 mm) and stretched from 0% to 120%. Reprinted with permission from ref. 307. Copyright © 2022, American Chemical Society. (d) The Kapton-GFET sensor is integrated with a miniaturised circuit for G-FET control and measurement. (e) Schematic of the solution-gated G-FET-based biosensor. (f) Zoomed-in view of the sensing area, showing aptamer-functionalized graphene for IL-6 biomarker targeting. Reprinted with permission from ref. 150. Copyright © 2022, Elsevier. (g) Diagrammatic sketch of the nanosensor, with the graphene-covered channel between the drain and source and a transparent electrode composed of 30 nm WO3, 8 nm Au, and 30 nm WO3. (h) Photograph of the nanosensor attached to the skin of fingertips and (i) to an artificial eye. Reprinted with permission from ref. 308. Copyright © 2022, John Wiley and Sons. (j) Schematic of the integrated diagnostic and therapeutic system for real-time monitoring and therapy of chronic ocular surface inflammation (OSI). (k) Photograph of a soft, smart contact lens (scale bar: 2 cm) with the inset showing a live rabbit wearing the lens (scale bar: 1 cm). (l) Photograph of a rabbit wearing a pair of AgNF-based heat patches on its upper and lower eyelids (scale bar: 2 cm). Reprinted under terms of CC-BY-NC 4.0 from ref. 309. Copyright © 2021, The American Association for the Advancement of Science.

nonspecific adsorption and endows the biosensor with regenerability. This biosensor can detect cytokine storm biomarkers, including IFN-γ, in undiluted human sweat with a lower bound for detection at 740 fM. Experimental results demonstrated that the biosensor maintained a consistent response during regeneration and wrinkling tests without mechanical damage, Fig. 16d. In addition, the same group engineered a wearable and deformable G-FET sensor on an ultrathin 2.5-μm-thick substrate with high mechanical durability.[304] The team employed wet transfer and lithography to deposit graphene and gold electrodes onto the substrate, Fig. 16 e-g. The biosensor detected inflammatory cytokines TNF-α and IFN-γ, with detection limits of 2.75 and 2.89 pM, respectively.

Building on this work, Hao *et al.* developed a dual-channel G-FET biosensor (Fig. 16h–j) enabling multiplex detection of biomarkers.[305] In this work, IFN-γ, TNF-α, and IL-6 in biological fluids were characterised in parallel. Hao *et al.* engineered another aptamer-based F-GFET sensor to rapidly detect hemoglobin in undiluted biological fluids.[307] The sensor uses PEI as a low-cost linking molecule to immobilise aptamers. The experimental results indicate that the graphene sensor modified with PEI can respond to changes in hemoglobin concentration within 6–8 min, with a minimal measurable quantity of 10.6 fM in 1× PBS, 14.2 fM in undiluted serum, and 11.9 fM in undiluted urine, respectively. The optimal PEI modification concentration was also determined to be 0.4 μM based on comparison experiments of hemoglobin detection in undiluted serum. Therefore, this sensor can potentially accurately monitor hemoglobin in a clinical setting, Fig. 17a–c.

Laliberte *et al.* fabricated a G-FET biosensor on a 25-μm-thick polyimide substrate, Fig. 17d–f.[310] By depositing a 50-nm-thick silicon dioxide (SiO_2) layer, graphene was transferred to a relatively flat surface to ensure its high mobility. The team demonstrated that the SiO_2 layer did not affect the flexibility of the biosensor, and coating the Kapton film with SiO_2 significantly improved the transconductance and consistency. Fig. 17g–i show an ultra-flexible and transparent wearable G-FET biosensor on a 1-μm-thick PET substrate as reported by Huang *et al.*[308] The biosensor was designed to detect body fluid biomarkers, focusing on L-cysteine. It detected L-cysteine in

undiluted human sweat and artificial tears with a sensitivity threshold of 0.022×10^{-6} M and 0.043×10^{-6} M, respectively. Considering its ultra-thin thickness and transparency, this F-GFET is expected to be used in applications such as contact lenses, which promotes the development of wearable biosensors in medical detection applications.

Jang *et al.* reported a pilot trial conducted on soft wearable contact lenses and an on-skin therapeutic device to simultaneously monitor and treat chronic ocular surface inflammation (OSI).[309] The innovative lenses are based on G-FETs to aid in continuously detecting the concentration of metalloproteinase-9 in tears for OSI diagnosis, Fig. 17j–l. When the level reaches a certain threshold, automated hyperthermia therapy is triggered by the therapeutic patches attached to the eyelids. These transparent patches are flexible and integrated with seamless communication with the contact lens and a smartphone, enabling timely diagnosis and treatment. The device has confirmed its efficiency and biocompatibility in *in-vivo* tests, proving its suitability as a non-invasive theranostic device.

Grand challenges and potential solutions

Graphene-based wearable devices showed great potential for providing non-invasive and sensitive detection of disease biomarkers. However, several challenges still exist and must be addressed before such devices can be fully implemented and commercialised. This necessitates more interdisciplinary research to develop innovative solutions.

Reusability and regeneration are significant challenges in wearables, as they are vital for real-time monitoring applications. Various strategies have been developed for reusing the immobilised biomolecules multiple times while maintaining their integrity and functionality, and switching the biochemical reactions with the target analyte on and off. However, the number of regenerations is limited, and maintaining the biomolecule function is still puzzling. Therefore, the enhancement of regeneration techniques like reversible binding chemistries, enzyme-assisted regeneration, and electrochemical desorption can help overcome this limitation to help extend the operational lifespan of the devices. For reliable, long-term use of biosensors, research is needed on regeneration protocols and durable biosensor architectures.

Another major significant challenge is the proper modification of bare graphene surfaces to establish a stable and sustainable bond with the bioreceptors of interest. For the detection of disease biomarkers, it is imperative to achieve high specificity and sensitivity through the efficient functionalisation of biomolecules. However, it remains unclear whether the induced chemical modification will remain stable under harsh conditions for a long time. To overcome this limitation, further research is needed to improve functionalisation techniques, including covalent coupling using SAMs and integrating protective coatings, to ensure the long-term stability of bound bioreceptors under wearable conditions.

Stability remains a significant challenge for graphene-based sensors. The performance of sensors can be adversely affected by environmental factors, including humidity and mechanical stress. For example, prolonged contact with sweat or skin may cause the graphene layers to delaminate or deteriorate. Therefore, sensors can be encapsulated with robust materials, including biocompatible polymers or advanced nanocomposites, to help mitigate the adverse effects of external impacts. Additionally, modifying graphene's chemical and structural properties through doping or functionalisation could enhance its performance under wearable conditions.

Current fabrication methods, including LIG and CVD, have many limitations regarding scalability. Even though laboratory-scale techniques produce high-quality sensors, translating them to large-scale mass production is challenging because of their high cost, reproducibility, and evolving complexity. Innovative approaches, such as roll-to-roll manufacturing and laser scribing, offer promise but need to be further optimised in order to achieve a balance between quality and cost. Combining graphene with other nanomaterials and hybrid fabrication techniques may open up new pathways for scalable sensor production.

Graphene-based biosensors are inconsistently reliable in clinical settings because they lack standardised guidelines for their performance and validation. Device discrepancies in terms of sensitivity, specificity, and accuracy in analyte detection might be attributed to variations in the fabrication techniques of materials, batch-to-batch variations, and testing protocols. Industry-wide benchmarks for sensor design, calibration, and testing must be established to achieve regulatory approval and ensure clinical adoption. Collaborative efforts between academia, industry, and regulatory bodies will be essential in creating standardised validation frameworks.

The current generation of graphene-based sensors primarily focuses on detecting single biomarkers. However, a broader range of biomarkers may allow a more comprehensive assessment of diseases and associated conditions. Accordingly, there is an increasing demand for multiplexed biosensors that can simultaneously track several parameters to provide a holistic picture of an individual's health, allowing for a more accurate and detailed understanding of disease physiology.

Future perspectives

The future of graphene-based wearable biosensors depends on the integration of the device into an intelligent, self-sustaining healthcare ecosystem. Next-generation devices must seamlessly merge high-performance miniaturised graphene sensing devices with advanced microfabrication, real-time wireless communication, and innovative data analysis pipelines to unlock their full potential.

Artificial intelligence (AI) and machine learning (ML) are poised to fundamentally reshape biosensor functionality by enabling real-time, adaptive interpretation of complex biomarker profiles. Instead of passively recording the sensor's data,

 This journal is © The Royal Society of Chemistry 2025

future graphene-based wearable sensors could actively learn from temporal trends, detect subtle pathophysiological deviations, and provide predictive alerts for conditions such as chronic stress, metabolic imbalance, or diseases at early stages. Beyond mere diagnosis, AI-assisted wearable platforms could evolve into personalised health management systems, offering dynamic risk assessments and recommending proactive interventions.

A transformative goal is the creation of closed-loop sensing-actuation systems. In this paradigm, graphene-based sensors continuously monitor key biomarkers and autonomously trigger therapeutic actions, such as drug release, neuromodulation, or environmental adjustments, based on real-time biochemical feedback. Graphene's extended surface area, mechanical resilience, and electrical and electrochemical properties uniquely position it as a perfectly suitable material for such intelligent platforms.

Integration into the Internet of Things (IoT) will further promote the overall capabilities of wearable biosensors, enabling distributed networks of physiological data that clinicians can monitor remotely. Real-time cloud-based analytics would facilitate early clinical intervention, personalised treatment adjustments, and decentralised healthcare models, mainly benefiting populations with limited access to medical facilities.

Concurrently, breakthroughs in self-powered systems will be critical for maintaining the long-term wearability of graphene devices. Energy harvesting technologies, such as biofuel cells exploiting sweat metabolites, thermoelectric generators utilising body heat, or piezoelectric systems harnessing motion, will allow biosensors to operate independently without reliance on conventional batteries, promoting fully autonomous, long-term physiological monitoring.

Realising these ambitions will require interdisciplinary collaboration across materials science, microelectronics, machine learning, clinical research, and regulatory sciences. Graphene-based wearable biosensors will transition from promising laboratory prototypes to indispensable tools for personalised, predictive, and preventative healthcare only through coordinated innovation at these interfaces.

By overcoming these scientific and engineering challenges, graphene-based integrated wearable sensors will redefine the concept of disease monitoring, shifting the paradigm from basic reactive treatments to intelligent, continuous, and seamless health monitoring. This will help improve healthcare management systems and patients' quality of life globally.

Conclusion

The present review discusses advances in wearable technology and the incorporation of graphene nanostructures into a wearable context, emphasising the importance of graphene nanostructures in mental health management. Exceptional electrical and chemical properties of graphene, coupled with its suitability for miniaturised microfluidic systems, allow for the development of non-invasive biosensors. Graphene devices combined with innovative signal transduction mechanisms provide sensitive and precise real-time monitoring of stress biomarkers, aligning with the growing demand for personalised healthcare. The advances addressed in this review highlight the importance of graphene-based wearables for reliable and sensitive monitoring solutions, thus contributing to enhanced stress management and quality of life.

Author contributions

M. A. A. drafted the original manuscript. S. S. J., N. K. and N. T. N. edited and revised the final manuscript. N. T. N. supervised the project.

Data availability

No primary research results, software or code have been included and no new data were generated or analysed as part of this review.

Conflicts of interest

There are no conflicts to declare.

Acknowledgements

The project is supported by the Australian Research Council through the Australian Laureate Fellowship (FL230100023) to N.T.N.

References

1 M. L. González Ramírez, J. P. García Vázquez, M. D. Rodríguez, L. A. Padilla-López, G. M. Galindo-Aldana and D. Cuevas-González, *Healthcare*, 2023, **11**, 2369.
2 S. M. A. Iqbal, I. Mahgoub, E. Du, M. Ann Leavitt and W. Asghar, *npj Flexible Electron.*, 2021, **5**, 9.
3 H. Seo, W. G. Chung, Y. W. Kwon, S. Kim, Y. M. Hong, W. Park, E. Kim, J. Lee, S. Lee, M. Kim, K. Lim, I. Jeong, H. Song and J. U. Park, *Chem. Rev.*, 2023, **123**(19), 11488–11558.
4 K. Lazaros, S. Adam, M. G. Krokidis, T. Exarchos, P. Vlamos and A. G. Vrahatis, *Sensors*, 2025, **25**, 1396.
5 S. S. Gambhir, T. J. Ge, O. Vermesh, R. Spitler and G. E. Gold, *Sci. Transl. Med.*, 2021, **13**, eabe5383.
6 J. R. Sempionatto, J. A. Lasalde-Ramírez, K. Mahato, J. Wang and W. Gao, *Nat. Rev. Chem.*, 2022, **6**, 899–915.
7 Y. Yang, Y. Song, X. Bo, J. Min, O. S. Pak, L. Zhu, M. Wang, J. Tu, A. Kogan, H. Zhang, T. K. Hsiai, Z. Li and W. Gao, *Nat. Biotechnol.*, 2020, **38**, 217–224.
8 F. Gao, C. Liu, L. Zhang, T. Liu, Z. Wang, Z. Song, H. Cai, Z. Fang, J. Chen, J. Wang, M. Han, J. Wang, K. Lin, R. Wang, M. Li, Q. Mei, X. Ma, S. Liang, G. Gou and N. Xue, *Microsyst. Nanoeng.*, 2023, **9**, 1.

9 S. Guo, K. Wu, C. Li, H. Wang, Z. Sun, D. Xi, S. Zhang, W. Ding, M. E. Zaghloul, C. Wang, F. A. Castro, D. Yang and Y. Zhao, *Matter*, 2021, **4**, 969–985.
10 H. Y. Y. Nyein, L. C. Tai, Q. P. Ngo, M. Chao, G. B. Zhang, W. Gao, M. Bariya, J. Bullock, H. Kim, H. M. Fahad and A. Javey, *ACS Sens.*, 2018, **3**, 944–952.
11 E. Liu, Z. Cai, Y. Ye, M. Zhou, H. Liao and Y. Yi, *Sensors*, 2023, **23**, 817.
12 X. Zhu, S. Yuan, Y. Ju, J. Yang, C. Zhao and H. Liu, *Anal. Chem.*, 2019, **91**, 10764–10771.
13 S. Zhang, Z. He, W. Zhao, C. Liu, S. Zhou, O. O. Ibrahim, C. Wang and Q. Wang, *Nanomaterials*, 2024, **14**, 857.
14 G. Maduraiveeran, M. Sasidharan and V. Ganesan, *Biosens. Bioelectron.*, 2018, **103**, 113–129.
15 S. Su, Q. Sun, X. Gu, Y. Xu, J. Shen, D. Zhu, J. Chao, C. Fan and L. Wang, *TrAC, Trends Anal. Chem.*, 2019, **119**, 115610.
16 M. Saleh, A. Gul, A. Nasir, T. O. Moses, Y. Nural and E. Yabalak, *J. Ind. Eng. Chem.*, 2025, **146**, 176–212.
17 Y. Ren, F. Zhang, Z. Yan and P. Y. Chen, *Device*, 2025, **3**, 100676.
18 A. Dube, S. J. Malode, A. N. Alodhayb, K. Mondal and N. P. Shetti, *Talanta Open*, 2025, **11**, 100395.
19 R. G. Ferreira, A. P. Silva and J. Nunes-Pereira, *ACS Sens.*, 2024, **9**, 1104–1133.
20 A. Baruah, R. Newar, S. Das, N. Kalita, M. Nath, P. Ghosh, S. Chinnam, H. Sarma and M. Narayan, *Discover Nano*, 2024, **19**, 1–29.
21 Y. Lei, T. Zhang, Y. C. Lin, T. Granzier-Nakajima, G. Bepete, D. A. Kowalczyk, Z. Lin, D. Zhou, T. F. Schranghamer, A. Dodda, A. Sebastian, Y. Chen, Y. Liu, G. Pourtois, T. J. Kempa, B. Schuler, M. T. Edmonds, S. Y. Quek, U. Wurstbauer, S. M. Wu, N. R. Glavin, S. Das, S. P. Dash, J. M. Redwing, J. A. Robinson and M. Terrones, *ACS Nanosci. Au*, 2022, **2**, 450–485.
22 J. J. Mim, M. Hasan, M. S. Chowdhury, J. Ghosh, M. H. Mobarak, F. Khanom and N. Hossain, *Heliyon*, 2024, **10**, e29244.
23 J. Li, H. Zeng, Z. Zeng, Y. Zeng and T. Xie, *ACS Biomater. Sci. Eng.*, 2021, **7**, 5363–5396.
24 T. Tene, S. Bellucci, F. Arias Arias, L. S. Carrera Almendariz, A. G. Flores Huilcapi and C. Vacacela Gomez, *Sensors*, 2024, **24**, 4670.
25 T. Bertaglia, T. J. Neubert, R. M. Iost, K. Balasubramanian and F. N. Crespilho, *Curr. Opin. Electrochem.*, 2024, 101641.
26 N. Chauhan, T. Maekawa and D. N. S. Kumar, *J. Mater. Res.*, 2017, **32**, 2860–2882.
27 X. Liu, M. Wang, L. Cao, J. Zhuang, D. Wang, M. Wu and B. Liu, *Adv. Mater.*, 2024, **36**, 2403355.
28 L. Yang and H. Wang, *Acta Biomater.*, 2024, **185**, 24–40.
29 S. Zhang, H. Zhou, R. Tchantchane and G. Alici, *IEEE/ASME Trans. Mechatron.*, 2025, **30**(1), 369–380.
30 J. Park, Y. Lee, S. Cho, A. Choe, J. Yeom, Y. G. Ro, J. Kim, D. H. Kang, S. Lee and H. Ko, *Chem. Rev.*, 2024, **124**, 1464–1534.
31 L. Q. Tao, H. Tian, Y. Liu, Z. Y. Ju, Y. Pang, Y. Q. Chen, D. Y. Wang, X. G. Tian, J. C. Yan, N. Q. Deng, Y. Yang and T. L. Ren, *Nat. Commun.*, 2017, **8**, 1–8.
32 R. S. Perala, N. Chandrasekar, R. Balaji, P. S. Alexander, N. Z. N. Humaidi and M. T. Hwang, *Mater. Sci. Eng., R*, 2024, **159**, 100805.
33 M. Sun, C. Zhang, S. Lu, S. Mahmood, J. Wang, C. Sun, J. Pang, L. Han and H. Liu, *Adv. Funct. Mater.*, 2024, **34**, 2405471.
34 Z. Ma, *Int. J. Electrochem. Sci.*, 2024, **19**, 100760.
35 S. Cheng, Z. Gu, L. Zhou, M. Hao, H. An, K. Song, X. Wu, K. Zhang, Z. Zhao, Y. Dong and Y. Wen, *Front. Bioeng. Biotechnol.*, 2021, **9**, 765987.
36 H. C. Ates, P. Q. Nguyen, L. Gonzalez-Macia, E. Morales-Narváez, F. Güder, J. J. Collins and C. Dincer, *Nat. Rev. Mater.*, 2022, **7**, 887–907.
37 J. S. Joymangul, I. Ciobanu, F. Agnoloni, J. Lampe, C. Pedrini, A. Pinto, B. Franceschini, D. Nicolas, E. Tamburini, F. Cecchi, M. Berteanu and D. Khadraoui, *Appl. Sci.*, 2024, **14**, 4789.
38 W. Wu, L. Li, Z. Li, J. Sun and L. Wang, *Adv. Mater.*, 2023, **35**, 2304596.
39 FreeStyle Libre Continuous Glucose Monitoring|FreeStyle Libre US, **https://www.freestyle.abbott/us-en/home.html**, (accessed 19 January 2025).
40 Introducing Dexcom G7|Dexcom, **https://www.dexcom.com/en-AU/dexcom-g7-cgm-system**, (accessed 19 January 2025).
41 GX Sweat Patch - Epicore Biosystems, **https://www.epicorebiosystems.com/our-solutions/gx-sweat-patch**, (accessed 19 January 2025).
42 Gx Sweat Patch (2-pack)|Gatorade Official Site, **https://www.gatorade.com/equipment/gx-sweat-patch/gx-sweat-patch-00052000048520**, (accessed 20 January 2025).
43 G. Quer, J. M. Radin, M. Gadaleta, K. Baca-Motes, L. Ariniello, E. Ramos, V. Kheterpal, E. J. Topol and S. R. Steinhubl, *Nat. Med.*, 2021, **27**, 73–77.
44 Y. Cotur, M. Kasimatis, M. Kaisti, S. Olenik, C. Georgiou and F. Güder, *Adv. Funct. Mater.*, 2020, **30**(16), 1910288.
45 T. Liu, K. Zhou, R. Ma, L. Zhang, C. Huang, Z. Luo, H. Zhu, S. Yao, C. Yang, B. Zou and L. Ye, *Aggregate*, 2023, **4**, e308.
46 C. J. Weber, O. M. Clay, R. E. Lycan, G. K. Anderson and O. Simoska, *Anal. Bioanal. Chem.*, 2023, **416**, 87–106.
47 S. M. Mugo, W. Lu and S. Robertson, *Biosensors*, 2022, **12**, 854.
48 S. M. Mugo, J. Alberkant, N. Bernstein and O. V. Zenkina, *Anal. Methods*, 2021, **13**, 4169–4173.
49 S. M. Mugo, W. Lu, M. Wood and S. Lemieux, *Electrochem. Sci. Adv.*, 2022, **2**, e2100039.
50 S. Demuru, J. Kim, M. El Chazli, S. Bruce, M. Dupertuis, P. A. Binz, M. Saubade, C. Lafaye and D. Briand, *ACS Sens.*, 2022, **7**, 2721–2731.
51 S. M. Mugo and J. Alberkant, *Anal. Bioanal. Chem.*, 2020, **412**, 1825–1833.
52 X. Wang, J. Zhou and H. Wang, *Cell Rep. Phys. Sci.*, 2024, **5**, 101801.
53 Y. Jia, S. Chen, Q. Wang and J. Li, *Nanoscale*, 2024, **16**, 2834–2846.
54 M. Wang, Y. Yang, J. Min, Y. Song, J. Tu, D. Mukasa, C. Ye, C. Xu, N. Heflin, J. S. McCune, T. K. Hsiai, Z. Li and W. Gao, *Nat. Biomed. Eng.*, 2022, **6**, 1225–1235.

 This journal is © The Royal Society of Chemistry 2025

55 M. Janghorban, I. Aradanas, S. Kazemi, P. Ngaju and R. Pandey, *Biosensors*, 2022, **12**, 986.
56 Q. Zhang, D. Jiang, C. Xu, Y. Ge, X. Liu, Q. Wei, L. Huang, X. Ren, C. Wang and Y. Wang, *Sens. Actuators, B*, 2020, **320**, 128325.
57 H. Park, W. Park and C. H. Lee, *NPG Asia Mater.*, 2021, **13**, 1–14.
58 O. Parlak, S. T. Keene, A. Marais, V. F. Curto and A. Salleo, *Sci. Adv.*, 2018, **4**(7), eaar2904.
59 D. Pérez and J. Orozco, *Microchim. Acta*, 2022, **189**, 1–28.
60 J. Min, J. R. Sempionatto, H. Teymourian, J. Wang and W. Gao, *Biosens. Bioelectron.*, 2021, **172**, 112750.
61 M. Garg, A. Parihar and M. S. Rahman, *Mater. Adv.*, 2024, **5**, 432–452.
62 N. K. Singh, S. Chung, A. Y. Chang, J. Wang and D. A. Hall, *Biosens. Bioelectron.*, 2023, **227**, 115097.
63 R. M. Torrente-Rodríguez, J. Tu, Y. Yang, J. Min, M. Wang, Y. Song, Y. Yu, C. Xu, C. Ye, W. W. IsHak and W. Gao, *Matter*, 2020, **2**, 921–937.
64 N. L. Kazanskiy, S. N. Khonina and M. A. Butt, *Sens. Actuators, A*, 2024, **366**, 114993.
65 C. D. Flynn, D. Chang, A. Mahmud, H. Yousefi, J. Das, K. T. Riordan, E. H. Sargent and S. O. Kelley, *Nat. Rev. Bioeng.*, 2023, **1**, 560–575.
66 R. He, H. Liu, Y. Niu, H. Zhang, G. M. Genin and F. Xu, *npj Flexible Electron.*, 2022, **6**, 1–11.
67 M. Friedel, I. A. P. Thompson, G. Kasting, R. Polsky, D. Cunningham, H. T. Soh and J. Heikenfeld, *Nat. Biomed. Eng.*, 2023, **7**, 1541–1555.
68 R. He, Y. Niu, Z. Li, A. Li, H. Yang, F. Xu and F. Li, *Adv. Healthcare Mater.*, 2020, **9**, 1901201.
69 P. Makvandi, M. Kirkby, A. R. J. Hutton, M. Shabani, C. K. Y. Yiu, Z. Baghbantaraghdari, R. Jamaledin, M. Carlotti, B. Mazzolai, V. Mattoli and R. F. Donnelly, *Nano-Micro Lett.*, 2021, **13**, 1–41.
70 A. Childs, B. Mayol, J. A. Lasalde-Ramírez, Y. Song, J. R. Sempionatto and W. Gao, *ACS Nano*, 2024, **18**, 24605–24616.
71 E. Lori Zoudani, N. T. Nguyen and N. Kashaninejad, *Small Struct.*, 2024, **5**, 2400121.
72 Y. Kim and M. R. Prausnitz, *Nat. Biomed. Eng.*, 2021, **5**, 3–5.
73 Y. Wu, F. Tehrani, H. Teymourian, J. Mack, A. Shaver, M. Reynoso, J. Kavner, N. Huang, A. Furmidge, A. Duvvuri, Y. Nie, L. M. Laffel, F. J. Doyle, M. E. Patti, E. Dassau, J. Wang and N. Arroyo-Currás, *Anal. Chem.*, 2022, **94**, 8335–8345.
74 K. Moussi, A. Bukhamsin, T. Hidalgo and J. Kosel, *Adv. Eng. Mater.*, 2020, **22**(2), 1901358.
75 Y. Hu, Z. Pan, M. De Bock, T. X. Tan, Y. Wang, Y. Shi, N. Yan and A. K. Yetisen, *Biosens. Bioelectron.*, 2024, **262**, 116542.
76 D. H. Lee, S. Lim, S. S. Kwak and J. Kim, *Adv. Healthcare Mater.*, 2024, **13**, 2302375.
77 M. R. Prausnitz, *Adv. Drug Delivery Rev.*, 1996, **18**, 395–425.
78 T. K. Giri, S. Chakrabarty and B. Ghosh, *J. Controlled Release*, 2017, **246**, 30–38.
79 M. Majdinasab, *Wearable Biosensing in Medicine and Healthcare*, 2024, 35–66.
80 A. J. Bandodkar, W. Jia, C. Yardimci, X. Wang, J. Ramirez and J. Wang, *Anal. Chem.*, 2015, **87**, 394–398.
81 G. Wang, N. Moriyama, S. Tottori and M. Nishizawa, *Mater. Today Bio*, 2025, **31**, 101504.
82 Y. Yao, J. Chen, Y. Guo, T. Lv, Z. Chen, N. Li, S. Cao, B. Chen and T. Chen, *Biosens. Bioelectron.*, 2021, **179**, 113078.
83 J. R. Sempionatto, A. A. Khorshed, A. Ahmed, A. N. De Loyola, E. Silva, A. Barfidokht, L. Yin, K. Y. Goud, M. A. Mohamed, E. Bailey, J. May, C. Aebischer, C. Chatelle and J. Wang, *ACS Sens.*, 2020, **5**, 1804–1813.
84 E. V. Karpova, E. V. Shcherbacheva, A. A. Galushin, D. V. Vokhmyanina, E. E. Karyakina and A. A. Karyakin, *Anal. Chem.*, 2019, **91**, 3778–3783.
85 N. G. Costa, J. C. Antunes, A. J. Paleo and A. M. Rocha, *Biosensors*, 2022, **12**, 252.
86 S. Emaminejad, W. Gao, E. Wu, Z. A. Davies, H. Y. Y. Nyein, S. Challa, S. P. Ryan, H. M. Fahad, K. Chen, Z. Shahpar, S. Talebi, C. Milla, A. Javey and R. W. Davis, *Proc. Natl. Acad. Sci. U. S. A.*, 2017, **114**, 4625–4630.
87 B. Jagannath, K. C. Lin, M. Pali, D. Sankhala, S. Muthukumar and S. Prasad, *Bioeng. Transl. Med.*, 2021, **6**(3), e10220.
88 B. Jagannath, K.-C. Lin, M. Pali, D. Sankhala, S. Muthukumar and S. Prasad, *Inflamm. Bowel Dis.*, 2020, **26**(10), 1533–1542.
89 N. Kodjo, M. Churcher, S. Upasham, P. Rice, S. Bhadsavle and S. Prasad, *RSC Adv.*, 2020, **10**, 23173–23186.
90 S. Kim, B. Lee, J. T. Reeder, S. H. Seo, S. U. Lee, A. Hourlier-Fargette, J. Shin, Y. Sekine, H. Jeong, Y. S. Oh, A. J. Aranyosi, S. P. Lee, J. B. Model, G. Lee, M. H. Seo, S. S. Kwak, S. Jo, G. Park, S. Han, I. Park, H. Il Jung, R. Ghaffari, J. Koo, P. V. Braun and J. A. Rogers, *Proc. Natl. Acad. Sci. U. S. A.*, 2020, **117**, 27906–27915.
91 S. Emaminejad, S. S. Emaminejad, H. Hojaiji, Y. Zhao, M. C. Gong, M. Mallajosyula, J. Tan, H. Lin, A. M. Hojaiji, S. Lin, C. Milla and A. M. Madni, *Lab Chip*, 2020, **20**, 4582–4591.
92 J. Kim, J. R. Sempionatto, S. Imani, M. C. Hartel, A. Barfidokht, G. Tang, A. S. Campbell, P. P. Mercier and J. Wang, *Adv. Sci.*, 2018, **5**(10), 1800880.
93 P. Q. Nguyen, L. R. Soenksen, N. M. Donghia, N. M. Angenent-Mari, H. De Puig, A. Huang, R. Lee, S. Slomovic, T. Galbersanini, G. Lansberry, H. M. Sallum, E. M. Zhao, J. B. Niemi and J. J. Collins, *Nat. Biotechnol.*, 2021, **39**, 1366–1374.
94 H. C. Ates, A. Brunauer, F. von Stetten, G. A. Urban, F. Güder, A. Merkoçi, S. M. Früh and C. Dincer, *Adv. Funct. Mater.*, 2021, **31**(15), 2010388.
95 H. C. Ates, P. Q. Nguyen, L. Gonzalez-Macia, E. Morales-Narváez, F. Güder, J. J. Collins and C. Dincer, *Nat. Res.*, 2022, **7**(11), 887–907.
96 T. Mishra, M. Wang, A. A. Metwally, G. K. Bogu, A. W. Brooks, A. Bahmani, A. Alavi, A. Celli, E. Higgs, O. Dagan-Rosenfeld, B. Fay, S. Kirkpatrick, R. Kellogg, M. Gibson, T. Wang, E. M. Hunting, P. Mamic,

A. B. Ganz, B. Rolnik, X. Li and M. P. Snyder, *Nat. Biomed. Eng.*, 2020, **4**, 1208–1220.
97 J. R. Sempionatto, V. R. V. Montiel, E. Vargas, H. Teymourian and J. Wang, *ACS Sens.*, 2021, **6**, 1745–1760.
98 S. Apoorva, N. T. Nguyen and K. R. Sreejith, *Lab Chip*, 2024, **24**, 1833–1866.
99 L. Paternò and L. Lorenzon, *Front. Robot. AI*, 2023, **10**, 1075634.
100 N. Mishra, N. T. Garland, K. A. Hewett, M. Shamsi, M. D. Dickey and A. J. Bandodkar, *ACS Sens.*, 2022, **7**, 3169–3180.
101 X. Hou, Y. S. Zhang, G. T. De Santiago, M. M. Alvarez, J. Ribas, S. J. Jonas, P. S. Weiss, A. M. Andrews, J. Aizenberg and A. Khademhosseini, *Nature Reviews Materials*, 2017, **2**, 1–15.
102 N. Kashaninejad and N. T. Nguyen, *Lab Chip*, 2023, **23**, 913–937.
103 C. Shi, Y. Zhao, P. Zhu, J. Xiao and G. Nie, *Smart Mater. Struct.*, 2021, **30**, 105001.
104 M. K. Filippidou, A. I. Kanaris, E. Aslanidis, A. Rapesi, D. Tsounidi, S. Ntouskas, E. Skotadis, G. Tsekenis, D. Tsoukalas, A. Tserepi and S. Chatzandroulis, *Micromachines*, 2023, **14**, 1595.
105 U. Mogera, H. Guo, M. Namkoong, M. S. Rahman, T. Nguyen and L. Tian, *Sci. Adv.*, 2022, **8**(12), eabn1736.
106 L. Milić, N. S. Zambry, F. B. Ibrahim, B. Petrović, S. Kojić, A. Thiha, K. Joseph, N. F. Jamaluddin and G. M. Stojanović, *Biomicrofluidics*, 2024, **18**(5), 051502.
107 R. Lin, H. J. Kim, S. Achavananthadith, Z. Xiong, J. K. W. Lee, Y. L. Kong and J. S. Ho, *Nat. Commun.*, 2022, **13**, 1–10.
108 B. Senf, W. H. Yeo and J. H. Kim, *Biosensors*, 2020, **10**, 127.
109 J. Wu, H. Liu, W. Chen, B. Ma and H. Ju, *Nat. Rev. Bioeng.*, 2023, **1**, 346–360.
110 J. Jyoti, R. Kaur, S. Rana and V. Kumar, *RSC Detect. Sci. Ser.*, 2024, **28**, 166–190.
111 Z. Zhang, J. J. Hu, S. Lin, J. Wu, F. Xia and X. Lou, *Interdiscip. Med.*, 2024, **2**, e20240032.
112 L. Hosseinzadeh and M. Mazloum-Ardakani, *Adv. Clin. Chem.*, 2020, **99**, 237–279.
113 Y. Seok Kim, N. H. Ahmad Raston and M. Bock Gu, *Biosens. Bioelectron.*, 2016, **76**, 2–19.
114 Z. Zheng, R. Zhu, I. Peng, Z. Xu and Y. Jiang, *J. Mater. Chem. B*, 2024, **12**, 8577–8604.
115 J. Wu, H. Liu, W. Chen, B. Ma and H. Ju, *Nat. Rev. Bioeng.*, 2023, **1**, 346–360.
116 Y. Tian, G. Xu, K. Cai, X. Zhao, B. Zhang, L. Wang and T. Wang, *Nanoscale*, 2022, **15**, 80–91.
117 H. Y. Y. Nyein, M. Bariya, B. Tran, C. H. Ahn, B. J. Brown, W. Ji, N. Davis and A. Javey, *Nat. Commun.*, 2021, **12**, 1–13.
118 K. Kaewpradub, K. Veenuttranon, H. Jantapaso, P. Mittraparparthorn and I. Jeerapan, *Nano-Micro Lett.*, 2025, **17**, 1–21.
119 Z. Xu, J. Song, B. Liu, S. Lv, F. Gao, X. Luo and P. Wang, *Sens. Actuators, B*, 2021, **348**, 130674.
120 X. T. Zheng, Z. Yang, L. Sutarlie, M. Thangaveloo, Y. Yu, N. A. B. Salleh, J. S. Chin, Z. Xiong, D. L. Becker, X. J. Loh, B. C. K. Tee and X. Su, *Sci. Adv.*, 2023, **9**(24), eadg6670.
121 D. Ciobanu, O. Hosu-Stancioiu, G. Melinte, F. Ognean, I. Simon and C. Cristea, *Biosensors*, 2023, **14**, 7.
122 H. Zhang, S. Ye, L. Huang, S. Fan, W. Mao, Y. Hu, Y. Yu and F. Fu, *Anal. Methods*, 2022, **15**, 99–108.
123 C. Fenzl, P. Nayak, T. Hirsch, O. S. Wolfbeis, H. N. Alshareef and A. J. Baeumner, *ACS Sens.*, 2017, **2**, 616–620.
124 J. Zhang, Y. Chai, R. Yuan, Y. Yuan, L. Bai, S. Xie and L. Jiang, *Analyst*, 2013, **138**, 4558–4564.
125 H. Lee, C. Song, Y. S. Hong, M. S. Kim, H. R. Cho, T. Kang, K. Shin, S. H. Choi, T. Hyeon and D. H. Kim, *Sci. Adv.*, 2024, **19**(1), 20220933.
126 Z. Štukovnik, R. Fuchs-Godec and U. Bren, *Biosensors*, 2023, **13**, 899.
127 C. Robinson, V. B. Juska and A. O'Riordan, *Environ. Res.*, 2023, **237**, 116877.
128 K. Vora, N. Kordas and K. Seidl, *Sensors*, 2023, **23**, 9696.
129 N. Sitkov, A. Ryabko, V. Moshnikov, A. Aleshin, D. Kaplun and T. Zimina, *Micromachines*, 2024, **15**, 181.
130 T. B. Tran, S. J. Son and J. Min, *BioChip J.*, 2016, **10**, 318–330.
131 H. S. Magar, R. Y. A. Hassan and A. Mulchandani, *Sensors*, 2021, **21**, 6578.
132 Y. S. Chen, C. H. Huang, P. C. Pai, J. Seo and K. F. Lei, *Biosensors*, 2023, **13**, 83.
133 N. Sitkov, A. Ryabko, V. Moshnikov, A. Aleshin, D. Kaplun and T. Zimina, *Micromachines*, 2024, **15**, 181.
134 R. D. Munje, S. Muthukumar and S. Prasad, *Sens. Actuators, B*, 2017, **238**, 482–490.
135 T. Yang, S. Wang, H. Jin, W. Bao, S. Huang and J. Wang, *Sens. Actuators, B*, 2013, **178**, 310–315.
136 J. Min, S. Demchyshyn, J. R. Sempionatto, Y. Song, B. Hailegnaw, C. Xu, Y. Yang, S. Solomon, C. Putz, L. E. Lehner, J. F. Schwarz, C. Schwarzinger, M. C. Scharber, E. Shirzaei Sani, M. Kaltenbrunner and W. Gao, *Nat. Electron.*, 2023, **6**, 630–641.
137 J. R. Sempionatto, M. Lin, L. Yin, E. De la paz, K. Pei, T. Sonsa-ard, A. N. de Loyola Silva, A. A. Khorshed, F. Zhang, N. Tostado, S. Xu and J. Wang, *Nat. Biomed. Eng.*, 2021, **5**, 737–748.
138 T. T. H. Nguyen, C. M. Nguyen, M. A. Huynh, H. H. Vu, T. K. Nguyen and N. T. Nguyen, *J. Nanobiotechnol.*, 2023, **21**, 1–29.
139 T. Wadhera, D. Kakkar, G. Wadhwa and B. Raj, *J. Electron. Mater.*, 2019, **48**, 7635–7646.
140 S. Cao, P. Sun, G. Xiao, Q. Tang, X. Sun, H. Zhao, S. Zhao, H. Lu and Z. Yue, *Electrochem. Sci. Adv.*, 2023, **3**, e2100207.
141 H. Li, D. Li, H. Chen, X. Yue, K. Fan, L. Dong and G. Wang, *Sensors*, 2023, **23**, 6808.
142 J. Wang, D. Ye, Q. Meng, C. An Di and D. Zhu, *Adv. Mater. Technol.*, 2020, **5**, 2000218.
143 Y. Ding, K. Tan, S. Zhang, S. Wang, X. Zhang and P. A. Hu, *Chem. Eng. J.*, 2023, **477**, 146844.
144 D. H. Kang, J. G. Choi, W. J. Lee, D. Heo, S. Wang, S. Park and M. H. Yoon, *APL Bioeng.*, 2023, **7**(2), 026102.
145 Q. Liu, C. Zhao, M. Chen, Y. Liu, Z. Zhao, F. Wu, Z. Li, P. S. Weiss, A. M. Andrews and C. Zhou, *iScience*, 2020, **23**, 101469.
146 B. Wang, C. Zhao, Z. Wang, K. A. Yang, X. Cheng, W. Liu, W. Yu, S. Lin, Y. Zhao, K. M. Cheung, H. Lin, H. Hojaiji,

 This journal is © The Royal Society of Chemistry 2025

P. S. Weiss, M. N. Stojanović, A. J. Tomiyama, A. M. Andrews and S. Emaminejad, *Sci. Adv.*, 2022, **8**(1), eabk0967.
147 M. Abrantes, D. Rodrigues, T. Domingues, S. S. Nemala, P. Monteiro, J. Borme, P. Alpuim and L. Jacinto, *J. Nanobiotechnol.*, 2022, **20**, 1–15.
148 G. Wu, N. Zhang, A. Matarasso, I. Heck, H. Li, W. Lu, J. G. Phaup, M. J. Schneider, Y. Wu, Z. Weng, H. Sun, Z. Gao, X. Zhang, S. G. Sandberg, D. Parvin, E. Seaholm, S. K. Islam, X. Wang, P. E. M. Phillips, D. C. Castro, S. Ding, D. P. Li, M. R. Bruchas and Y. Zhang, *Nano Lett.*, 2022, **22**, 3668–3677.
149 R. Zhang and Y. Jia, *ACS Sens.*, 2021, **6**, 3024–3031.
150 K. E. Laliberte, P. Scott, N. I. Khan, M. S. Mahmud and E. Song, *Microelectron. Eng.*, 2022, **262**, 111835.
151 P. Govindaraj, A. Mirabedini, X. Jin, D. Antiohos, N. Salim, P. Aitchison, J. Parker, F. K. Fuss and N. Hameed, *J. Mater. Sci. Technol.*, 2023, **155**, 10–32.
152 J. Lin, Z. Peng, Y. Liu, F. Ruiz-Zepeda, R. Ye, E. L. G. Samuel, M. J. Yacaman, B. I. Yakobson and J. M. Tour, *Nat. Commun.*, 2014, **5**, 1–8.
153 R. Ye, D. K. James, J. M. Tour, R. Ye, D. K. James and M. Tour, *Adv. Mater.*, 2019, **31**, 1803621.
154 A. A. Lahcen, S. Rauf, T. Beduk, C. Durmus, A. Aljedaibi, S. Timur, H. N. Alshareef, A. Amine, O. S. Wolfbeis and K. N. Salama, *Biosens. Bioelectron.*, 2020, **168**, 112565.
155 Y. Chyan, R. Ye, Y. Li, S. P. Singh, C. J. Arnusch and J. M. Tour, *ACS Nano*, 2018, **12**, 2176–2183.
156 S. P. Singh, Y. Li, J. Zhang, J. M. Tour and C. J. Arnusch, *ACS Nano*, 2018, **12**, 289–297.
157 X. Han, R. Ye, Y. Chyan, T. Wang, C. Zhang, L. Shi, T. Zhang, Y. Zhao and J. M. Tour, *ACS Appl. Nano Mater.*, 2018, **1**, 5053–5061.
158 L. Huang, J. Su, Y. Song and R. Ye, *Nano-Micro Lett.*, 2020, **12**, 1–17.
159 A. R. Cardoso, A. C. Marques, L. Santos, A. F. Carvalho, F. M. Costa, R. Martins, M. G. F. Sales and E. Fortunato, *Biosens. Bioelectron.*, 2019, **124–125**, 167–175.
160 A. F. Carvalho, A. J. S. Fernandes, C. Leitão, J. Deuermeier, A. C. Marques, R. Martins, E. Fortunato, F. M. Costa, A. F. Carvalho, A. J. S. Fernandes, C. Leitão, F. M. Costa, J. Deuermeier, A. C. Marques, R. Martins and E. Fortunato, *Adv. Funct. Mater.*, 2018, **28**, 1805271.
161 K. S. Novoselov, A. K. Geim, S. V. Morozov, D. Jiang, Y. Zhang, S. V. Dubonos, I. V. Grigorieva and A. A. Firsov, *Science*, 2004, **306**, 666–669.
162 J. Plutnar, M. Pumera and Z. Sofer, *J. Mater. Chem. C*, 2018, **6**, 6082–6101.
163 L. González-Rodríguez, S. Pérez-Davila, M. López-Álvarez, S. Chiussi, J. Serra and P. González, *J. Nanobiotechnol.*, 2023, **21**, 1–12.
164 R. R. A. Soares, R. G. Hjort, C. C. Pola, K. Parate, E. L. Reis, N. F. F. Soares, E. S. Mclamore, J. C. Claussen and C. L. Gomes, *ACS Sens.*, 2020, **5**, 1900–1911.
165 A. C. Bressi, A. Dallinger, Y. Steksova and F. Greco, *ACS Appl. Mater. Interfaces*, 2023, **15**, 35788–35814.
166 H. R. Moon and B. Ryu, *Int. J. Precision Eng. Manuf. – Green Technol.*, 2024, **11**, 1279–1294.
167 H. Wang, Z. Zhao, P. Liu and X. Guo, *Biosensors*, 2022, **12**, 55.
168 W. S. Hummers, Jr. and R. E. Offeman, *J. Am. Chem. Soc.*, 1958, **80**(6), 1339.
169 D. C. Marcano, D. V. Kosynkin, J. M. Berlin, A. Sinitskii, Z. Sun, A. Slesarev, L. B. Alemany, W. Lu and J. M. Tour, *ACS Nano*, 2010, **4**, 4806–4814.
170 S. Fang, Y. Lin and Y. H. Hu, *ACS Sustainable Chem. Eng.*, 2019, **7**, 12671–12681.
171 A. Gosai, K. R. Khondakar, X. Ma and M. A. Ali, *Biosensors*, 2021, **11**, 384.
172 M. Pandey, R. Nazar, M. H. A. Elella, S. Praharaj, E. Makhado, D. Rout and E. H. Gilani, *Bionanoscience*, 2024, **15**, 1–33.
173 V. Agarwal and P. B. Zetterlund, *Chem. Eng. J.*, 2021, **405**, 127018.
174 M. Kurian, *Carbon Trends*, 2021, **5**, 100120.
175 K. K. H. De Silva, H. H. Huang, R. Joshi and M. Yoshimura, *Carbon*, 2020, **166**, 74–90.
176 N. Bellier, P. Baipaywad, N. Ryu, J. Y. Lee and H. Park, *Biomater. Res.*, 2022, **26**, 1–23.
177 J. A. Quezada Renteria, C. Ruiz-Garcia, T. Sauvage, L. F. Chazaro-Ruiz, J. R. Rangel-Mendez and C. O. Ania, *Phys. Chem. Chem. Phys.*, 2020, **22**, 20732–20743.
178 M. Fatkullin, D. Cheshev, A. Averkiev, A. Gorbunova, G. Murastov, J. Liu, P. Postnikov, C. Cheng, R. D. Rodriguez and E. Sheremet, *Nat. Commun.*, 2024, **15**, 1–13.
179 S. Rani, S. Singh and B. Pal, *Int. J. Hydrogen Energy*, 2024, **49**, 910–924.
180 Z. Luo, D. Yang, J. Liu, H. Y. Zhao, T. Zhao, B. X. Li, W. G. Yang and Z. Z. Yu, *Adv. Funct. Mater.*, 2023, **33**, 2212032.
181 A. Hamed, A. Hessein and A. Abd El-Moneim, *Appl. Surf. Sci.*, 2021, **551**, 149457.
182 S. P. Singh, Y. Li, J. Zhang, J. M. Tour and C. J. Arnusch, *ACS Nano*, 2018, **12**, 289–297.
183 Z. Wan, M. Umer, M. Lobino, D. Thiel, N. T. Nguyen, A. Trinchi, M. J. A. Shiddiky, Y. Gao and Q. Li, *Carbon*, 2020, **163**, 385–394.
184 N. Kumar, P. K. Sahoo, S. Y. Lee and S. J. Park, *Sustainable Mater. Technol.*, 2024, **40**, e00962.
185 R. Kumar, R. Pandey, E. Joanni and R. Savu, *Chem. Eng. J.*, 2024, **497**, 154968.
186 S. Aftab, G. Koyyada, M. Mukhtar, F. Kabir, G. Nazir, S. A. Memon, M. Aslam, M. A. Assiri and J. H. Kim, *ACS Sens.*, 2024, **9**(9), 4536–4554.
187 A. Singh, A. Shi and S. A. Claridge, *Chem. Commun.*, 2022, **58**, 13059–13070.
188 Y. Zhang, H. Yu, L. Wang, X. Wu, J. He, W. Huang, C. Ouyang, D. Chen and B. E. Keshta, *Adv. Colloid Interface Sci.*, 2024, **329**, 103197.
189 Y. Z. N. Htwe and M. Mariatti, *J. Sci.: Adv. Mater. Devices*, 2022, **7**, 100435.
190 Y. C. Goswami and S. Begzaad, *Energy Storage*, 2024, **6**, e666.
191 X. Han, X. Lin, Y. Sun, L. Huang, F. Huo and R. Xie, *ACS Appl. Mater. Interfaces*, 2024, **16**, 55010.

192 R. Wei, H. Li, Z. Chen, Q. Hua, G. Shen and K. Jiang, *npj Flexible Electron.*, 2024, **8**, 1–20.
193 J. R. J, J. T. Mazumder, A. B. Aloshious and R. K. Jha, *Nanoscale*, 2025, **17**, 11960–12013.
194 J. Seong, Y. Jeon, Y. Yang, T. Badloe and J. Rho, *Int. J. Precision Eng. Manuf. – Green Technol.*, 2023, **11**, 685–706.
195 K. Karimi, A. Fardoost, N. Mhatre, J. Rajan, D. Boisvert and M. Javanmard, *Micromachines*, 2024, **15**, 1274.
196 A. A. Manshina, I. I. Tumkin, E. M. Khairullina, M. Mizoshiri, A. Ostendorf, S. A. Kulinich, S. Makarov, A. A. Kuchmizhak and E. L. Gurevich, *Adv. Funct. Mater.*, 2024, **34**, 2405457.
197 K. P. R. Castro, R. N. P. Colombo, R. M. Iost, B. G. R. da Silva and F. N. Crespilho, *Anal. Bioanal. Chem.*, 2023, **415**, 3879–3895.
198 M. Kong, M. Yang, R. Li, Y. Z. Long, J. Zhang, X. Huang, X. Cui, Y. Zhang, Z. Said and C. Li, *Int. J. Adv. Manuf. Technol.*, 2023, **131**, 3205–3237.
199 L. Zhu, J. Hao, B. Xu and B. Wang, *Int. J. Adv. Manuf. Technol.*, 2022, **121**, 6049–6057.
200 F. Ershad, S. Patel and C. Yu, *npj Flexible Electron.*, 2023, **7**, 1–15.
201 A. Bashiri, M. J. Large, M. J. Griffith, L. Papale, B. Philippa, C. Hall, D. Bolst, S. Guatelli, A. J. Mozer, M. Petasecca and J. A. Posar, *Adv. Funct. Mater.*, 2024, **35**, 2415723.
202 T. Zhang, Y. Chai, S. Wang, J. Yu, S. Jiang, W. Zhu, Z. Fang and B. Li, *Sensors*, 2023, **23**, 9743.
203 P. K. Sharma and J. Y. Chung, *Micromachines*, 2023, **14**, 735.
204 S. Kumar, R. Singh, A. P. Singh and Y. Wei, *Proc. Inst. Mech. Eng., Part L*, 2023, **237**, 1678–1692.
205 D. Luo, H. Sun, Q. Li, X. Niu, Y. He and H. Liu, *ACS Sens.*, 2023, **8**, 465–481.
206 Y. Xing, J. Wang and J. Li, *Int. J. Extreme Manuf.*, 2024, **6**, 062005.
207 S. Kim, J. Kang, I. Lee, J. Jang, C. B. Park, W. Lee and B. S. Bae, *npj Flexible Electron.*, 2023, **7**, 1–9.
208 M. Hu, K. Zhu, J. Wei, K. Yang, L. Wu, S. Zong and Z. Wang, *Biosens. Bioelectron.*, 2024, **265**, 116662.
209 F. Lin and W. Cheng, *Adv. Electron. Mater.*, 2023, **9**, 2300334.
210 S. Fan, W. Chang, C. Fei, Z. Zhang, B. Hou, Z. Shi, H. Wang and Y. Hui, *Cellulose*, 2022, **29**, 8919–8935.
211 D. A. Dikin, S. Stankovich, E. J. Zimney, R. D. Piner, G. H. B. Dommett, G. Evmenenko, S. T. Nguyen and R. S. Ruoff, *Nature*, 2007, **448**, 457–460.
212 L. Gong, I. A. Kinloch, R. J. Young, I. Riaz, R. Jalil and K. S. Novoselov, *Adv. Mater.*, 2010, **22**, 2694–2697.
213 I. Singh, A. K. Rehni, P. Kumar, M. Kumar and H. Y. Aboul-Enein, *Fullerenes, Nanotubes Carbon Nanostruct.*, 2009, **17**, 361–377.
214 Z. Han, J. Wang, S. Liu, Q. Zhang, Y. Liu, Y. Tan, S. Luo, F. Guo, J. Ma, P. Li, X. Ming, C. Gao and Z. Xu, *Adv. Fiber Mater.*, 2022, **4**, 268–279.
215 W. Meng, M. Nie, Z. Liu and J. Zhou, *Adv. Fiber Mater.*, 2021, **3**, 149–159.
216 Z. Wu, X. Li, Z. Feng, C. Wan, Y. Li, T. Li, Q. Yang, X. Liu, M. Ren, J. Li, X. Shang, X. Zhang and X. Huang, *Adv. Healthcare Mater.*, 2023, **12**, 2202629.
217 K. Zhao, J. Han, Y. Ma, Z. Tong, J. Suhr, M. Wang, L. Xiao, S. Jia and X. Chen, *Nanomaterials*, 2023, **13**, 701.
218 M. Owais, A. Shiverskii, A. K. Pal, B. Mahato and S. G. Abaimov, *Polymers*, 2022, **14**, 4796.
219 Q. Zhang, Q. Wei, K. Huang, Z. Liu, W. Ma, Z. Zhang, Y. Zhang, H. M. Cheng and W. Ren, *Natl. Sci. Rev.*, 2023, **10**(7), nwad147.
220 G. Liu, Z. Lv, S. Batool, M. Z. Li, P. Zhao, L. Guo, Y. Wang, Y. Zhou and S. T. Han, *Small*, 2023, **19**, 2207879.
221 M. Akter, H. R. Anik, S. I. Tushar, I. S. Tania, Md. K. H. Chowdhury, S. Md. M. Hasan and B. F. Bristy, *Adv. Sens. Res.*, 2024, **3**, 2300120.
222 P. Govindaraj, A. Mirabedini, X. Jin, D. Antiohos, N. Salim, P. Aitchison, J. Parker, F. K. Fuss and N. Hameed, *J. Mater. Sci. Technol.*, 2023, **155**, 10–32.
223 U. D'Amora, S. Dacrory, M. S. Hasanin, A. Longo, A. Soriente, S. Kamel, M. G. Raucci, L. Ambrosio and S. Scialla, *Pharmaceutics*, 2023, **15**, 338.
224 M. Hosseini Hooshiar, A. Mozaffari, M. Hamed Ahmed, R. Abdul Kareem, A. Jaber Zrzo, A. Salah Mansoor, Z. H. Athab, Z. Parhizgar and P. Amini, *Biomed. Eng. Online*, 2024, **23**, 1–45.
225 T. Thaweeskulchai, K. Sakdaphetsiri and A. Schulte, *Microchim. Acta*, 2024, **191**, 1–30.
226 M. Mohkam, M. Sadraeian, A. Lauto, A. Gholami, S. H. Nabavizadeh, H. Esmaeilzadeh and S. Alyasin, *Microsyst. Nanoeng.*, 2023, **9**, 1–23.
227 H. Lin, T. Buerki-Thurnherr, J. Kaur, P. Wick, M. Pelin, A. Tubaro, F. C. Carniel, M. Tretiach, E. Flahaut, D. Iglesias, E. Vázquez, G. Cellot, L. Ballerini, V. Castagnola, F. Benfenati, A. Armirotti, A. Sallustrau, F. Taran, M. Keck, C. Bussy, S. Vranic, K. Kostarelos, M. Connolly, J. M. Navas, F. Mouchet, L. Gauthier, J. Baker, B. Suarez-Merino, T. Kanerva, M. Prato, B. Fadeel and A. Bianco, *ACS Nano*, 2024, **18**, 6038–6094.
228 A. Sharma, M. Badea, S. Tiwari and J. L. Marty, *Molecules*, 2021, **26**, 748.
229 T. Zahra, U. Javeria, H. Jamal, M. M. Baig, F. Akhtar and U. Kamran, *Anal. Chim. Acta*, 2024, **1316**, 342880.
230 S. Majumder, A. K. Roy, T. Mondal and M. Jamal Deen, *IEEE J. Flexible Electron.*, 2025, **4**(2), 63–88.
231 R. Kumar, D. P. Singh, R. Muñoz, M. Amami, R. K. Singh, S. Singh and V. Kumar, *Mater. Today Chem.*, 2023, **33**, 101750.
232 N. Singh, D. S. Dkhar, P. Chandra and U. P. Azad, *Biosensors*, 2023, **13**, 166.
233 L. Li, T. Wang, Y. Zhong, R. Li, W. Deng, X. Xiao, Y. Xu, J. Zhang, X. Hu and Y. Wang, *J. Mater. Chem. B*, 2024, **12**, 1168–1193.
234 M. Bilal, E. Ullah Rashid, J. Zdarta and T. Jesionowski, *Chem. Eng. J.*, 2023, **452**, 139509.
235 S. Dhanraj, S. Sundaresh and A. K. Saikumar, *J. Electrochem. Soc.*, 2023, **169**, 120536.

 This journal is © The Royal Society of Chemistry 2025

236 N. Kumari, M. Bhandari, N. Kumari and M. Bhandari, *Chemistry of Graphene – Synthesis, Reactivity, Applications and Toxicities*, 2024, DOI: 10.5772/INTECHOPEN.114855.
237 M. S. K. Chowdury, Y. J. Park, S. B. Park and Y. il Park, *Sustainable Mater. Technol.*, 2024, **42**, e01124.
238 Abid, P. Sehrawat, S. S. Islam, P. Mishra and S. Ahmad, *Sci. Rep.*, 2018, **8**(1), 3537.
239 J. Narayan and K. Bezborah, *RSC Adv.*, 2024, **14**, 13413–13444.
240 F. Junge, M. Auge, Z. Zarkua and H. Hofsäss, *Nanomaterials*, 2023, **13**, 658.
241 V. Manikandan and N. Y. Lee, *Chemosphere*, 2023, **311**, 136934.
242 W. Yu, L. Sisi, Y. Haiyan and L. Jie, *RSC Adv.*, 2020, **10**, 15328–15345.
243 M. A. Khan, A. Kumar, J. Zhang and M. Kumar, *J. Mater. Chem. C*, 2021, **9**, 8129–8157.
244 S. Mukherjee, A. Mukherjee, Z. Bytesnikova, A. M. Ashrafi, L. Richtera and V. Adam, *Biosens. Bioelectron.*, 2024, **250**, 116050.
245 C. K. Chua and M. Pumera, *ACS Nano*, 2015, **9**, 4193–4199.
246 A. Mukherjee, A. M. Ashrafi, Z. Bytesnikova, P. Svec, L. Richtera and V. Adam, *J. Electroanal. Chem.*, 2023, **935**, 117301.
247 H. Ren, E. Cunha, Z. Li, L. Wang, I. A. Kinloch, D. Yi, A. Kretinin, Q. Sun, Z. Fan and R. J. Young, *J. Mater. Sci.*, 2022, **57**, 2683–2696.
248 R. Ziółkowski, A. Uścińska, M. Mazurkiewicz-Pawlicka, A. Małolepszy and E. Malinowska, *Electrochim. Acta*, 2019, **305**, 329–337.
249 C. Gao, M. Guo, Y. Liu, D. Zhang, F. Gao, L. Sun, J. Li, X. Chen, M. Terrones and Y. Wang, *Carbon*, 2023, **212**, 118133.
250 J. Zhan, Z. Lei and Y. Zhang, *Chem*, 2022, **8**, 947–979.
251 H. Bi, J. Liu, L. Wang, T. Liu, Z. Zhang, Q. Shen and S. Hayase, *eScience*, 2024, 100329.
252 J. Jang, G. D. Kong and H. J. Yoon, *Acc. Mater. Res.*, 2024, **5**(10), 1251–1262.
253 A. Tarasov, D. W. Gray, M. Y. Tsai, N. Shields, A. Montrose, N. Creedon, P. Lovera, A. O'Riordan, M. H. Mooney and E. M. Vogel, *Biosens. Bioelectron.*, 2016, **79**, 669–678.
254 D. Shin, H. R. Kim and B. H. Hong, *Nanoscale Adv.*, 2021, **3**, 1404–1412.
255 M. Ku, J. Kim, J. E. Won, W. Kang, Y. G. Park, J. Park, J. H. Lee, J. Cheon, H. H. Lee and J. U. Park, *Sci. Adv.*, 2020, **6**(28), eabb2891.
256 I. A. Isaac, N. Zine, M. Sigaud, P. Lozano-Sanchez, M. Caffio and A. Errachid, *Biosens. Bioelectron.*, 2023, **222**, 114954.
257 P. Song, C. S. Suchand Sangeeth, D. Thompson, W. Du, K. Ping Loh, C. A. Nijhuis, P. Song, C. S. S. Sangeeth, W. Du, K. P. Loh, C. A. Nijhuis and D. Thompson, *Adv. Mater.*, 2016, **28**, 631–639.
258 L. Xie, L. You and X. Cao, *Spectrochim. Acta, Part A*, 2013, **109**, 110–115.
259 O. P. Gomes, S. Kim, P. N. Lisboa-Filho, A. Batagin-Neto, Y. De Koninck and Y. Messaddeq, *J. Mater. Chem. C*, 2024, **12**, 6816–6825.
260 C. H. Chu, I. Sarangadharan, A. Regmi, Y. W. Chen, C. P. Hsu, W. H. Chang, G. Y. Lee, J. I. Chyi, C. C. Chen, S. C. Shiesh, G. Bin Lee and Y. L. Wang, *Sci. Rep.*, 2017, **7**, 1–15.
261 V. Georgakilas, J. N. Tiwari, K. C. Kemp, J. A. Perman, A. B. Bourlinos, K. S. Kim and R. Zboril, *Chem. Rev.*, 2016, **116**, 5464–5519.
262 S. Balaban, T. Beduk, C. Durmus, E. Aydindogan, K. N. Salama and S. Timur, *Electroanalysis*, 2021, **33**, 1072–1080.
263 C. Fenzl, P. Nayak, T. Hirsch, O. S. Wolfbeis, H. N. Alshareef and A. J. Baeumner, *ACS Sens.*, 2017, **2**, 616–620.
264 M. J. Treanor, P. Lozano-Sanchez, Y. Bunga, R. Schaub and M. Caffio, *Appl. Surf. Sci.*, 2025, **680**, 161426.
265 Z. Hao, Y. Zhu, X. Wang, P. G. Rotti, C. Dimarco, S. R. Tyler, X. Zhao, J. F. Engelhardt, J. Hone and Q. Lin, *ACS Appl. Mater. Interfaces*, 2017, **9**, 27504–27511.
266 Z. Hao, Y. Pan, W. Shao, Q. Lin and X. Zhao, *Biosens. Bioelectron.*, 2019, **134**, 16–23.
267 D. Kwong Hong Tsang, T. J. Lieberthal, C. Watts, I. E. Dunlop, S. Ramadan, A. E. del Rio Hernandez and N. Klein, *Sci. Rep.*, 2019, **9**, 1–10.
268 S. C. Barman, M. Ali, E. A. Hasan, N. Wehbe, H. N. Alshareef and D. Alsulaiman, *ACS Mater. Lett.*, 2024, **6**, 837–846.
269 S. Khetani, V. Ozhukil Kollath, V. Kundra, M. D. Nguyen, C. Debert, A. Sen, K. Karan and A. Sanati-Nezhad, *ACS Sens.*, 2018, **3**, 844–851.
270 N. I. Khan and E. Song, *Sensors*, 2021, **21**, 1335.
271 Y. Nan, D. Gomez-Maldonado, K. Zhang, H. Du, D. C. Whitehead, M. Li, X. Zhang and M. S. Peresin, *Carbohydr. Polym. Technol. Appl.*, 2024, **8**, 100585.
272 F. R. Nitu, J. S. Burns and M. Ionită, *Coatings*, 2020, **10**, 420.
273 Y. U. Kim and W. J. Cho, *Biosensors*, 2024, **14**, 141.
274 G. Rabost-Garcia, V. Colmena, J. Aguilar-Torán, J. Vieyra Galí, J. Punter-Villagrasa, J. Casals-Terré, P. Miribel-Catala, X. Muñoz, J. Cadefau, J. Padullés and D. Brotons Cuixart, *ACS Sens.*, 2023, **8**, 1536–1541.
275 M. A. Alam, *Biosens. Bioelectron. X*, 2024, **20**, 100515.
276 P. Ruengpirasiri, P. Charoensin, A. Aniwattapong, P. Natekuekool, C. Srisomwat, C. Pinyorospathum, S. Chaiyo and A. Yakoh, *ACS Omega*, 2024, **9**, 1634–1642.
277 S. Szunerits, T. Rodrigues, R. Bagale, H. Happy, R. Boukherroub and W. Knoll, *Anal. Bioanal. Chem.*, 2024, **416**, 2137–2150.
278 H. Teymourian, M. Parrilla, J. R. Sempionatto, N. F. Montiel, A. Barfidokht, R. Van Echelpoel, K. De Wael and J. Wang, *ACS Sens.*, 2020, **5**, 2679–2700.
279 E. R. Mamleyev, S. Heissler, A. Nefedov, P. G. Weidler, N. Nordin, V. V. Kudryashov, K. Länge, N. Mackinnon and S. Sharma, *npj Flexible Electron.*, 2019, **3**, 2.
280 X. Hui, X. Xuan, J. Kim and J. Y. Park, *Electrochim. Acta*, 2019, **328**, 135066.
281 Z. Wan, M. Umer, M. Lobino, D. Thiel, N.-T. Nguyen, A. Trinchi, M. J. Shiddiky, Y. Gao and Q. Li, *Carbon*, 2020, **163**, 385–394.

282 S. Chandra Barman, M. Abu Zahed, M. Sharifuzzaman, S. Gyu Ko, H. Yoon, J. San Nah, X. Xuan, J. Yeong Park, S. C. Barman, M. A. Zahed, S. G. Ko, H. Yoon, J. S. Nah, X. Xuan and J. Y. Park, *Adv. Funct. Mater.*, 2020, **30**, 1907297.

283 Y. Yang, Y. Song, X. Bo, J. Min, O. S. Pak, L. Zhu, M. Wang, J. Tu, A. Kogan, H. Zhang, T. K. Hsiai, Z. Li and W. Gao, *Nat. Biotechnol.*, 2019, **38**, 217–224.

284 T. Beduk, D. Beduk, J. Ilton De Oliveira Filho, F. Zihnioglu, C. Cicek, R. Sertoz, B. Arda, T. Goksel, K. Turhan, K. N. Salama and S. Timur, *Anal. Chem.*, 2021, **93**, 8585–8594.

285 M. Parrilla, I. Ortiz-Gómez, R. Cánovas, A. Salinas-Castillo, M. Cuartero and G. A. Crespo, *Anal. Chem.*, 2019, **91**, 8644–8651.

286 M. Garg, H. Guo, E. Maclam, E. Zhanov, S. Samudrala, A. Pavlov, M. S. Rahman, M. Namkoong, J. P. Moreno and L. Tian, *ACS Appl. Mater. Interfaces*, 2024, **16**, 46113–46122.

287 G. Xu, Z. A. Jarjes, V. Desprez, P. A. Kilmartin and J. Travas-Sejdic, *Biosens. Bioelectron.*, 2018, **107**, 184–191.

288 J. Zhu, S. Liu, Z. Hu, X. Zhang, N. Yi, K. Tang, M. G. Dexheimer, X. Lian, Q. Wang, J. Yang, J. Gray and H. Cheng, *Biosens. Bioelectron.*, 2021, **193**, 956–5663.

289 Y. Lei, A. H. Alshareef, W. Zhao and S. Inal, *ACS Appl. Nano Mater.*, 2019, **3**, 1166–1174.

290 M. Wang, Y. Yang, J. Min, Y. Song, J. Tu, D. Mukasa, C. Ye, C. Xu, N. Heflin, J. S. McCune, T. K. Hsiai, Z. Li and W. Gao, *Nat. Biomed. Eng.*, 2022, **6**, 1225–1235.

291 J. Tu, J. Min, Y. Song, C. Xu, J. Li, J. Moore, J. Hanson, E. Hu, T. Parimon, T. Y. Wang, E. Davoodi, T. F. Chou, P. Chen, J. J. Hsu, H. B. Rossiter and W. Gao, *Nat. Biomed. Eng.*, 2023, **7**, 1293–1306.

292 R. R. A. Soares, R. G. Hjort, C. C. Pola, K. Parate, E. L. Reis, N. F. F. Soares, E. S. Mclamore, J. C. Claussen and C. L. Gomes, *ACS Sens.*, 2020, **5**, 1900–1911.

293 S. C. Barman, M. Ali, E. A. Hasan, N. Wehbe, H. N. Alshareef and D. Alsulaiman, *ACS Mater. Lett.*, 2024, **6**, 837–846.

294 X. Xuan, H. S. Yoon and J. Y. Park, *Biosens. Bioelectron.*, 2018, **109**, 75–82.

295 Y. Shu, T. Su, Q. Lu, Z. Shang, Q. Xu and X. Hu, *Anal. Chem.*, 2021, **93**, 16222–16230.

296 X. Chen, X. Yan, J. Qiu, X. Zhang, Y. Zhang, H. Zhou, Y. Zhao, L. Han and Y. Zhang, *Sens. Diagn.*, 2024, **3**, 1724–1732.

297 I. Jeerapan, J. R. Sempionatto, A. Pavinatto, J. M. You and J. Wang, *J. Mater. Chem. A*, 2016, **4**, 18342–18353.

298 O. S. Kwon, S. J. Park, J. Y. Hong, A. R. Han, J. S. Lee, J. S. Lee, J. H. Oh and J. Jang, *ACS Nano*, 2012, **6**, 1486–1493.

299 C. Ju, Q. Fan and Y. Jia, Proceedings of the 2015 International Conference on Materials, Environmental and Biological Engineering, 2015, vol. 10, pp. 429–432.

300 S. Farid, X. Meshik, M. Choi, S. Mukherjee, Y. Lan, D. Parikh, S. Poduri, U. Baterdene, C.-E. Huang, Y. Y. Wang, P. Burke, M. Dutta and M. A. Stroscio, *Biosens. Bioelectron.*, 2015, **71**, 294–299.

301 Y. Yang, X. Yang, X. Zou, S. Wu, D. Wan, A. Cao, L. Liao, Q. Yuan and X. Duan, *Adv. Funct. Mater.*, 2017, **27**(19), 1604096.

302 Z. Wang, Z. Hao, S. Yu, C. G. De Moraes, L. H. Suh, X. Zhao and Q. Lin, *Adv. Funct. Mater.*, 2019, **29**(44), 1905202.

303 Z. Wang, Z. Hao, X. Wang, C. Huang, Q. Lin, X. Zhao and Y. Pan, *Adv. Funct. Mater.*, 2021, **31**(4), 2005958.

304 Z. Wang, Z. Hao, S. Yu, C. Huang, Y. Pan and X. Zhao, *Nanomaterials*, 2020, **10**, 1503.

305 Z. Hao, Y. Luo, C. Huang, Z. Wang, G. Song, Y. Pan, X. Zhao and S. Liu, *Small*, 2021, **17**, 2101508.

306 Z. Hao, Z. Wang, Y. Li, Y. Zhu, X. Wang, C. G. De Moraes, Y. Pan, X. Zhao and Q. Lin, *Nanoscale*, 2018, **10**, 21681–21688.

307 Z. Hao, C. Huang, C. Zhao, A. Kospan, Z. Wang, F. Li, H. Wang, X. Zhao, Y. Pan and S. Liu, *ACS Appl. Bio Mater.*, 2022, **5**, 1624–1632.

308 C. Huang, Z. Hao, Z. Wang, H. Wang, X. Zhao and Y. Pan, *Adv. Mater. Technol.*, 2022, **7**, 2101131.

309 J. Jang, J. Kim, H. Shin, Y. G. Park, B. J. Joo, H. Seo, J. E. Won, D. W. Kim, C. Y. Lee, H. K. Kim and J. U. Park, *Sci. Adv.*, 2021, **7**, 7194–7225.

310 K. E. Laliberte, P. Scott, N. I. Khan, S. Mahmud and E. Song, *Microelectron. Eng.*, 2022, **262**, 111835.

 This journal is © The Royal Society of Chemistry 2025